Check for updates

Received: 15 July 2020 | Revised: 12 November 2020 | Accepted: 13 December 2020

DOI: 10.1002/rnc.5394

RESEARCH ARTICLE

WILEY

A new actuator fault-tolerant control for Lipschitz nonlinear system using adaptive sliding mode control strategy

Salman Ijaz[1,2] | **Fuyang Chen**[2] | **Mirza Tariq Hamayun**[3]

[1]Department of Electrical and Electronics Engineering, University of Nottingham (UNNC), Ningbo, China

[2]College of Automation Engineering, Nanjing University of Aeronautics and Astronautics, Nanjing, China

[3]Department of Electrical and Computer Engineering, COMSATS University Islamabad, Lahore Campus, Lahore, Pakistan

Correspondence
Fuyang Chen, College of Automation Engineering, Nanjing University of Aeronautics and Astronautics, Nanjing, China.
Email: chenfuyang@nuaa.edu.cn

Abstract

This article proposed a new adaptive integral sliding mode (ISM) based fault-tolerant control (FTC) strategy to solve the actuator's faults and failures compensation problem for the class of Lipschitz nonlinear systems. A nominal state feedback virtual control law is designed first to stabilize the Lipschitz nonlinear system and to attain the desired nominal performance. To cater for the effect of faults and failures, the control allocation (CA) scheme reorganizes the virtual input signals among the healthy redundant actuators based on actuator's effectiveness level. Then, a nonlinear adaptive integral sliding mode controller (ISMC) is incorporated with the CA scheme to compensate for unknown disturbance and uncertainties effect that arises in the system by virtue of actuator faults/failures and error in fault estimation . An effective synthesis procedure is adopted to ensure the closed-loop stability condition using linear matrix inequality (LMI) optimization. Finally, the FTC scheme is tested to achieve maneuvering control of coaxial octorotor unmanned aerial vehicle (UAV) system. Simulations are performed on the nonlinear system at different actuator faults/failures combinations. Moreover, the effect of wind-gust, parameter variations, estimated state feedback and sensor noise are considered in nonlinear simulations. Finally, the results obtained during faults/failures are compared with the nominal condition and fixed ISMC based CA scheme.

KEYWORDS

adaptive control, fault tolerant control, linear matrix inequality, nonlinear control, sliding mode control

1 | INTRODUCTION

Fault-tolerant control (FTC) has gained a great deal of interest in the research community in recent years. The reason is increasing demand in reliability and safety needs in today's industrial systems, mainly in life-critical systems such as spacecraft, passenger aircraft, UAV's, nuclear and chemical plants. FTC is expected to tolerate actuator faults/failures, sensor faults/failures, and component faults/failures while maintaining system stability and desired performance.

Generally, FTC schemes are classified into active FTC (AFTC) and passive FTC (PFTC) schemes. PFTC technique provides robustness against the presumed faults. This approach neither required the fault estimation scheme nor the

 © 2021 John Wiley & Sons Ltd.

control reconfiguration at each fault step.[1-4] Although the PFTC scheme is restrictive to only a limited class of faults or failures, however, still in practice due to less time delay in response to the fault. AFTC scheme, on the other hand, responds to failures/failures based on the actuator efficiency information. However, the critical issues in any AFTC scheme are the efficient management of actuator's redundancy when prompt to faults/failures, ensure the system stability, and fulfillment of desired performance. Based on these issues, the design objectives include: (1) an efficient fault estimation scheme that perceives the fault information accurately, (2) consider a new control law or reconfigure the existing control law that can account for the stability of faulty system, and (3) the robustness against the uncertainty due to faults/failures and estimation error. The accomplishment of these design objectives requires not only the variation of controller parameters but also the structure of the controller (i.e., controller order, number, and type) might be changed.

AFTC schemes have been extensively studied for the linear invariant time (LTI) and linear parameter varying (LPV) class of systems in recent years. Various methods have been proposed to deal with actuator fault/failure, such as the re-configurable pseudo-inverse controller is designed in Reference 5 to handle actuator faults in the UAV system, where the change in parameters of control distribution matrix due to fault is identified using extended Kalman filter. The authors in Reference 6 suggested a combination of LMI and adaptive technique to handle the mismatch uncertainty and actuator faults. In Reference 7, an observer-based H_∞ FTC scheme is proposed to handle both the sensor and actuator faults. In Reference 8, linear quadratic regular (LQR) based model reference adaptive controller (MRAC) is designed to deal with the parameter variation and actuator failure due to vertical tail damaged aircraft. Some recent results on the FTC strategy belong to the class of the LPV system are obtained in References 9-12. CA scheme is considered an effective strategy to deal with actuator faults/failures specifically when sufficient redundant actuators are available in the system. In the past, the CA problem without considering fault/failure is intensively studied in Reference 13. However, in case of fault/failure, redistribution of virtual control signals among the set of available actuators, is required to ensure system performance which is known as a re-configurable CA problem. In conjunction with the re-configurable FTC, the authors in References 14 and 15 introduced the concept of CA and control reallocation for aircraft FTC. More results on the CA scheme for aircraft systems are obtained in Reference 16-18 which suggested the partitioning of full rank input matrix such that dominant contributions of control action are assigned to the states associated with an angular acceleration of roll, pitch, and yaw. To attain such partitioning of the input matrix is a complex process and involves several transformations. However, a recent proposed CA scheme in Reference 19 based on the singular value decomposition(SVD) of the input distribution matrix is relatively easier to perform and requires no state transformation. No doubt, the CA scheme is an effective method to manage actuator redundancy, but the uncertainty/external disturbance can affect the efficiency of the CA scheme which can detract from the precise system response. Therefore, the robust high-level controller is required to incorporate with the CA module. Among the various high-level controllers, sliding mode control (SMC) is an effective robust technique and is widely used within the FTC framework. SMC technique provides insensitivity against the model disturbance/uncertainty in the sliding phase.[20] Therefore, the integration of SMC with the CA scheme not only enhances the capability of handling the actuator failure issue but also provides robustness against model disturbance/uncertainties. Some recent results on the SMC-based CA scheme are proposed in References 16 and 21 for the class of uncertain LTI systems. For the class of affine LPV system, the authors in References 16,22,23, and 24 proposed SMC based CA scheme to deal with actuators faults and failures and has been applied successfully to civil aircraft and octorotor UAV systems. No doubt SMC provides robustness to the system response, but in the sliding phase, the system might get affected by the disturbance and uncertainty. On the other hand, integral SMC (ISMC) provides various advantages over SMC including elimination of reaching phase. Moreover, the un-matched term is also ameliorated with an appropriate choice of the sliding surface. In the existing work,[18,25,26] the ISMC scheme is also integrated with the CA unit to deal with total actuator failure issues of civil aircraft. In SMC/ISMC schemes, the main hurdle in practical implementation is high gain associated with discontinuous control that results in chattering. To cope with higher gain, the authors in References 20,27, and 28 proposed adaptive SMC/ISMC schemes in which sliding gain varies proportionally to the disturbance/uncertainty effect. The adaptive-ISMC based CA scheme is also proposed recently in References 25 and 29 to deal with the actuator's faults and failures.

The problem of robust stabilization of Lipschitz nonlinear system has received considerable attention in the past years.[30-33] In the real world, many practical systems satisfy the Lipschitz condition either globally or at least locally. The authors in Reference 30 first proposed necessary and sufficient conditions to ensure the asymptotic stability of Lipschitz nonlinear observer. Later on, in References 32 and 34, the results are extended to the design of an observer-based state feedback controller. The closed-loop system stability is guaranteed based on the separation principle, and LMI optimization is used to compute the controller gains. In Reference 35, a robust H_∞ controller is designed for the Lipschitz

10991239, 2021, 6, Downloaded from https://onlinelibrary.wiley.com/doi/10.1002/rnc.5394 by University Of Maryland, Wiley Online Library on [05/03/2024]. See the Terms and Conditions (https://onlinelibrary.wiley.com/terms-and-conditions) on Wiley Online Library for rules of use; OA articles are governed by the applicable Creative Commons License

nonlinear system to achieve the system stabilization. In the context of the FTC scheme for a class of Lipschitz nonlinear systems, several notable results have been obtained recently. Such as in Reference 36, a mixed H_2/H_∞ based FTC scheme is proposed that simultaneously estimate system states, and the fault-tolerant controller is designed using LMI optimization technique in the presence of noise/disturbance. In Reference 37, a virtual actuator approach is suggested to deal with actuator fault in the Lipschitz nonlinear system. The authors in Reference 38 presented a robust adaptive FTC scheme for Lipschitz nonlinear system to deal with actuator faults, bounded matched, and unmatched uncertainty. The adaptive strategy is integrated with a fixed state feedback controller to asymptotically stabilize the closed-loop system subject to the actuator's faults and disturbance effect. In Reference 39, H_∞ observer-based FTC scheme is considered that can estimate the system-states and faults accurately despite the disturbance effect. The system stability is guaranteed after a short transient time. Recently, in Reference 40, an adaptive sliding mode based FTC scheme for Lipschitz nonlinear system is proposed that effectively deals with sensor and actuator faults estimated by sliding mode observer (SMO).

In view of the remarkable benefits of the ISMC over SMC and the sufficient gap in the field of FTC for the class of over-actuated uncertain Lipschitz nonlinear system, this study proposed a new FTC scheme that integrates CA scheme with the ISMC and adaptive strategy. The proposed adaptive-ISMC based CA scheme was not previously considered for the class of Lipschitz nonlinear system to the best of the authors' knowledge. In the proposed method, the sufficient/necessary conditions are first derived to ensure the stability of the Lipschitz nonlinear system using the virtual control law in fault-free condition. Then the LQR problem is incorporated to synthesize the virtual control input signals to achieve the desired performance. In the face of faults/failures in any actuator, the CA scheme reroutes the control input signals to the healthy redundant actuators. The control reallocation is attained based on the perceived information from the fault estimation unit. To cope up with CA transient surge (due to low-rank approximation of input matrix), unknown disturbance/uncertainty, and fault estimation error, an adaptive-ISMC law is merged with virtual nominal control law such that required virtual control signals are available to CA scheme. The closed-loop stability of an uncertain Lipschitz nonlinear system is proven using the small gain theorem. and stability conditions are incorporated into the LMI framework. The proposed method is applied to a nonlinear octorotor UAV system. To implement FTC law, first, the nonlinear states equations are segregated into inner-loop over-actuated attitude and altitude state vector and outer-loop un-actuated position axes state vector. The proposed FTC method is utilized to acquire inner-loop control. Whereas for outer-loop (internal dynamics) stabilization and position tracking, a robust SMC based NDI control law is designed. The information of actuator effectiveness is obtained using the adaptive fault estimation scheme proposed in Reference 41. Compared to the recent results SMC based FTC scheme,[16-19,21,24-26,41] the main contributions are as follows.

- Compared to ISMC based CA schemes in References 16-19,21,25, and 41 based on LTI system and in References 24 and 26 for LPV system, this article considers Lipschitz nonlinear system to exploit adaptive-ISMC based FTC law.
- A detailed closed-loop stability analysis is performed subject to actuator's faults and failures, input matrix approximation error, unknown disturbance or uncertainty, and fault estimation error. The closed-loop stability is proven using small gain theorem and stability conditions are incorporated into LMI framework.
- In contrast with the existing adaptive-ISMC approaches in References 41 and 42, the proposed adaptive strategy increases the modulation gain only when the state trajectories cross the prescribed threshold value of the sliding surface. However, the modulation gain returns to the lowest prescribed value when the sliding movement enters into the neighborhood of the sliding surface. As a consequence, the undesirable chattering is reduced significantly.
- The proposed actuator FTC scheme is applied to achieve maneuvering control of the coaxial octorotor system. A detailed analysis is performed on a nonlinear system during actuator's faults/failures by considering several real-time flight conditions such as the wind-gust, parameter uncertainties, sensor/measurement noise, and estimated state information.

2 | PROBLEM FORMULATION

This section formulates the new FTC strategy for over-actuated Lipschitz nonlinear systems that integrates the ISMC law with CA scheme and adaptive strategy. The controller aims to keep the nominal performance despite the faults, failures, fault-estimation error, and external disturbance/uncertainty.

10991239, 2021, 6, Downloaded from https://onlinelibrary.wiley.com/doi/10.1002/rnc.5394 by University Of Maryland, Wiley Online Library on [05/03/2024]. See the Terms and Conditions (https://onlinelibrary.wiley.com/terms-and-conditions) on Wiley Online Library for rules of use; OA articles are governed by the applicable Creative Commons License

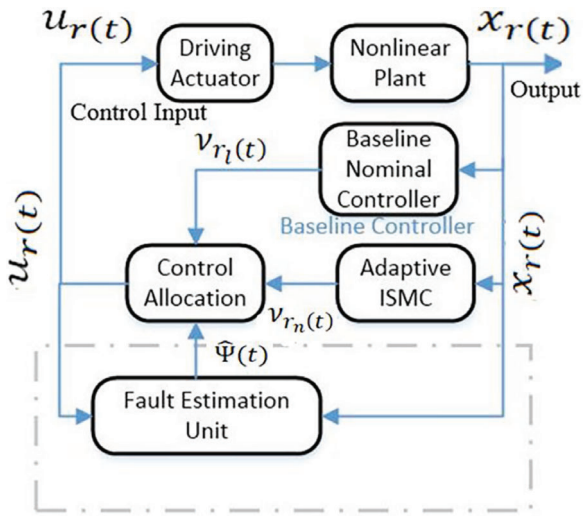

FIGURE 1 Architecture of overall control strategy [Colour figure can be viewed at wileyonlinelibrary.com]

Consider an over-actuated Lipschitz nonlinear system subject to the actuator's faults/failures and the disturbance/uncertainty defined as

$$\begin{cases} \dot{x}_r(t) = A_r x_r(t) + g_r(x_r, u_r, t) + B_r \Psi(t) u_r(t) + D_r \Phi_r(x_r, t) \\ y_r(t) = C_r x_r(t) \end{cases} \tag{1}$$

where $x_r(t) \in \Re^{n_r}$ denotes system state vector, $u_r(t) \in \Re^{m_r}$ is the control input vector, and $y_r(t) \in \Re^{l_r}$ shows the system output vector, respectively, with $l_r < min(m_r, n_r)$. The matrix $A_r \in \Re^{n_r \times n_r}$ belongs to the system matrix and is assumed to be fixed, $B_r \in \Re^{n_r \times m_r}$ is the control input distribution matrix, $C_r \in \Re^{l_r \times n_r}$ denotes the system output matrix, $D_r \in \Re^{n_r \times q_r}$ is the disturbance matrix, $\Phi_r(x_r, t) \in \Re^{q_r}$ is the disturbance input whose actual value is unknown but worst-case norm bounded and the diagonal matrix $\Psi(t) := diag(\psi_1(t), \psi_2(t), ..., \psi_{m_r}(t)) \in \Re^{m_r \times m_r}$ denotes the actuator's effectiveness level with the diagonal entries $\psi_1(t)....\psi_{m_r}(t)$ that specifically show individual actuator effectiveness. Specifically, the range $0 < \psi_i(t) < 1$ shows the faulty i^{th} actuator; the value $\psi_i = 0$ corresponds to failed actuator and $\psi_i = 1$ determines that the i^{th} actuator is fault free. The nonlinear function $g_r(x_r, u_r, t) \in \Re^{n_r}$ satisfies the Lipschitz condition, globally or at-least locally in the region $\mathcal{D}$, with respect to state $x_r(t)$ with the Lipschitz constant γ_{x_r}, that is,

$$\begin{cases} \|g_r(x_{r_1}, u_r, t) - g_r(x_{r_2}, u_r, t)\| \le \gamma_{x_r} \|x_{r_1} - x_{r_2}\| \\ g_r(0, u_r, t) = 0 \\ \forall x_{r_1}, x_{r_2} \in \Re^+ \quad \text{(globally Lipschitz)} \\ \forall x_{r_1}, x_{r_2} \in \mathcal{D} \quad \text{(locally Lipschitz)} \end{cases} \tag{2}$$

where $\|.\|$ is induced-2 norm and $t \in \Re^+$. The parameter γ_{x_r} is the Lipschitz constant and is defined as $\gamma_{x_r} = \sup_{x_r(t) \in \Re^{n_r}} \|\frac{\partial g_r}{\partial x_r}\|$.[43] Many nonlinear functions fulfill the Lipschitz condition either globally or at least locally.[31] For example, the trigonometric non-linearity in robotics system and the nonlinearities that are cubic or square in nature satisfy the Lipschitz condition.[36] The control architecture is shown in Figure 1. The aim is to design the actual control law $u_r(t)$ that translates virtual control signals $v_r(t)$, designed specifically using adaptive-ISMC technique, into actual actuator commands in the presence of faults, failures, fault estimation error, and external disturbance/uncertainty.

Prior to the control law development, the assumptions and useful lemma are described below that will be used throughout this article.

Assumption 1. The matrix B_r is assumed to be full rank, that is, $rank(B_r) = m_r$.

Assumption 2. It is assumed that the uncertainty term $\Phi_r(x_r, t)$ can be written into the form $\Phi_r(x_r, t) = \Phi_{r_{eq}}(t, x_r) x_r(t)$ and $\|\Phi_{r_{eq}}(t, x_r)\| \le \overline{\Phi}_{r_{eq}}$, where $\overline{\Phi}_{r_{eq}}$ denotes bound on uncertainty term.

10991239, 2021, 6, Downloaded from https://onlinelibrary.wiley.com/doi/10.1002/rnc.5394 by University Of Maryland, Wiley Online Library on [05/03/2024]. See the Terms and Conditions (https://onlinelibrary.wiley.com/terms-and-conditions) on Wiley Online Library for rules of use; OA articles are governed by the applicable Creative Commons License

Remark 1. In this article, we considered the class of system whose input distribution matrix is full-rank. Because in many actuator redundant systems such as aircraft system, the rank-deficient condition is not satisfied.[17,18] Therefore, in this work, the FTC synthesis procedure is carried out based on a full-rank input matrix. However, the proposed strategy can also be applied to a rank-deficient input matrix

Remark 2. Assumption 2 shows that the disturbance or uncertainty can be written as a linear-combination of system states and the disturbance function. Such an assumption is common for some physical plants. For example, in the aircraft system, the drag forces are the function of the aircraft velocity vector, which can be obtained into the linear -combination form as given in Assumption 2. The significance of this form is to simplify the closed-loop system analysis. It can also be seen disturbance term associated with the altitude, roll, pitch, and yaw rate of nonlinear model of octorotor UAV's (66) satisfies Assumption 2. Also, this assumption is being made in the existing works on FTC schemes.[18,41]

Lemma 1 (37). *For any $x_r, y_r \in \Re^{n_r}$ and a positive definite matrix $P_r \in \Re^{n_r \times n_r}$, the following inequality holds*

$$2x_r^T y_r \leq x_r^T P_r x_r + y_r^T P_r^{-1} y_r. \tag{3}$$

2.1 | CA scheme

To resolve the actuator redundancy, consider a SVD of input distribution matrix B_r defined as

$$B_r = \mathbb{U}_r \Sigma \mathbb{V}_r \tag{4}$$

where $\mathbb{U}_r \in \Re^{n_r \times n_r}$ and $\mathbb{V}_r \in \Re^{m_r \times m_r}$ are left and right singular matrices of B_r and are orthogonal. The matrix $\Sigma \in \Re^{m_r \times n_r}$ is a rectangular diagonal matrix where the non-negative diagonal entries $(\sigma_{r_1}, ..., \sigma_{r_{m_r}})$ are singular values of B_r and are sorted as, that is, $\sigma_{r_1} \geq \sigma_{r_2} ... \geq \sigma_{r_{m_r}}$. Next, approximate the matrix B_r to low-rank l_r, that is, B_{l_r} such that $rank(B_{l_r}) = l_r$. By using the low-rank approximation lemma given in Reference 44, the low rank l_r approximation of B_r in spectral norm is

$$B_{l_r} = \sum_{i=1}^{l_r} \sigma_{r_i} u_{r_i} v_{r_i}^T \tag{5}$$

where u_{r_i} and v_{r_i} are the ith column of $\mathbb{U}_r$ and $\mathbb{V}_r$, respectively. It can be shown that

$$\|B_r - B_{l_r}\| = \sum_{i=l_r+1}^{m_r} \|\sigma_{r_i} u_{r_i} v_{r_i}^T\|. \tag{6}$$

Now the rank of B_{l_r} is $l_r < m_r$, therefore B_{l_r} can be further factorized as $B_{l_r} = B_{l_1} B_{l_2}$ where $B_{l_1} \in \Re^{n_r \times l_r}$ and $B_{l_2} \in \Re^{l_r \times m_r}$ and both have full rank, that is, $rank(B_{l_1}) = rank(B_{l_2}) = l_r$. Finally the B_r matrix in (1) can be written as

$$B_r = B_{l_1} B_{l_2} + B_\delta \tag{7}$$

where $B_\delta = B_r - B_{l_r} \in \Re^{n_r \times m_r}$ is the approximation error. The partitioning of B_r in (7) ensures $B_{l_2} B_{l_2}^T = I_{l_r}$ and $\|B_{l_2}\| = I_{l_r}$.

Remark 3. In the literature, most of the existing work is being focused on low-rank input matrix where B_r can easily be factorized into $B_r = B_{l_1} B_{l_2}$ if $rank(B_r) = l_r < n_r$ where $B_{l_1} \in \Re^{n_r \times l_r}$ & $B_{l_2} \in \Re^{l_r \times m_r}$. However, if B_r is full rank, the authors in[16-18] suggested to reorder the states to the form $B_r = [B_1^T \; B_2^T]^T$, where $B_1 \in \Re^{(n_r - l_r) \times m_f}$ and $B_2 \in \Re^{l_r \times m_r}$. The state reordering to present more control input signal to the channel B_2 as compared to the channel B_1 and states scaling to make form $B_2 B_2^T = I_{l_r}$ are the complicated process especially for nonlinear systems. However, the partitioning of B_r using SVD and low rank approximation lemma is comparatively easier to perform and can be applied to both the full-rank and low-rank input matrices.[19]

Based on the partitioning of B_r in (7), the CA scheme is now defined to redistribute the virtual control signals among the set of available actuators based on the estimate of actuator effectiveness. A fault estimation unit provides an estimate

10991239, 2021, 6, Downloaded from https://onlinelibrary.wiley.com/doi/10.1002/rnc.5394 by University Of Maryland, Wiley Online Library on [05/03/2024]. See the Terms and Conditions (https://onlinelibrary.wiley.com/terms-and-conditions) on Wiley Online Library for rules of use; OA articles are governed by the applicable Creative Commons License

of the actuator's effectiveness and will be discussed in the sequential. However, in the control law development, the estimated information $\hat{\Psi}(t) \in \Re^{m_r \times m_r}$ is used and is defined as

$$\hat{\Psi}(t) = \text{diag}(\hat{\psi}_1(t), ..., \hat{\psi}_{m_r}(t)) \tag{8}$$

where the scalars terms $\hat{\psi}_i(t)$, $i = 1 \ldots m_r$ expressed the individual's effectiveness level. The estimation scheme will be provided later in this article. Since the perfect estimation is not practically possible, therefore certain level of estimation error is introduced and is defined as

$$\Psi(t) = (1 - \Delta(t))\hat{\Psi}(t) \tag{9}$$

where the estimation error $\Delta(t) \in \Re^{m_r \times m_r}$ is expressed as

$$\Delta(t) = \text{diag}(\delta_1(t), ..., \delta_{m_r}(t)) \tag{10}$$

where the scalar terms $\delta_1(t), ...\delta_{m_r}(t)$ denote the imperfection level in the estimated information. Next, the virtual control law $v_r(t) \in \Re^{l_r}$ based on l_r actuators is defined as

$$v_r(t) = B_{l_2} u_r(t). \tag{11}$$

The actual control signals $u_r(t)$ transmitted to the available set of actuators is obtained using (11) as

$$u_r(t) = B_{l_2}^{\dagger}(t) v_r(t) \tag{12}$$

where $B_{l_2}^{\dagger}(t)$ constitutes of weighted right pseudo-inverse of B_{l_2}. The choice of $B_{l_2}^{\dagger}(t)$ brings some design privilege in term of control signals distribution among the physical set of actuators. This design freedom is utilized by various researchers in the different ways. However, a generic choice of $B_{l_2}^{\dagger}(t)$, that is, $B_{l_2} B_{l_2}^{\dagger}(t) = I_{l_r}$ is

$$B_{l_2}^{\dagger}(t) = \hat{\Psi}(t) B_{l_2}^T (B_{l_2} \hat{\Psi}(t) B_{l_2}^T)^{-1} \tag{13}$$

where $\det(B_{l_2} \hat{\Psi}(t) B_{l_2}^T) \neq 0$ even up to $m_r - l_r$ entries of $\hat{\psi}_i(t) = 0$. However, in some special case the matrix $\hat{\Psi}(t)$ can contain more than $m_r - l_r$ zero entries, then $\det(B_{l_2} \hat{\Psi}(t) B_{l_2}^T) = 0$. Therefore a possible set of actuators faults and failures that the proposed FTC strategy can tolerate is expressed as

$$\overline{\Psi} = \{(\hat{\psi}_1(t), ...\hat{\psi}_{m_r}(t)) \in \underbrace{\begin{bmatrix} 0 & 1 \end{bmatrix} \times ..... \times \begin{bmatrix} 0 & 1 \end{bmatrix}}_{m_r} : det(B_{l_2} \hat{\Psi}(t) B_{l_2}^T \neq 0)\}. \tag{14}$$

Remark 4. When the perfect estimation is available and there is no faults and failures in the system, that is, $(\hat{\Psi}(t) = \Psi(t) = I_{m_r}$ & $\Delta(t) = 0)$, then $B_{l_2}^{\dagger}(t) = B_{l_2}^T$. The actual control signal $u_r(t)$ in (12) is obtained as

$$u_r(t) = B_{l_2}^T v_r(t). \tag{15}$$

Hence in fault-free condition, the virtual control input is translated to the actual input using the matrix $B_{l_2}^T$.

When the system is exposed to actuators faults/failures, and the estimation is not perfectly available, then the uncertain closed-loop system is attained by substituting (7), (9), and (12)-(13) into (1) which gives

$$\begin{aligned} \dot{x}_r(t) &= A_r x_r(t) + (B_{l_1} B_{l_2} + B_\delta)(1 - \Delta(t))\hat{\Psi}^2(t) B_{l_2}^T (B_{l_2} \hat{\Psi}(t) B_{l_2}^T)^{-1} v_r(t) + D_r \Phi_r(x_r, t) + g_r(x_r, u_r, t) \\ &= A_r x_r(t) + \underbrace{(B_{l_1} B_{l_2} + B_\delta)(1 - \Delta(t)) B_{l_2}^{+}(t) v_r(t)}_{\hat{B}_r(t)} + D_r \Phi_r(x_r, t) + g_r(x_r, u_r, t) \end{aligned} \tag{16}$$

10991239, 2021, 6, Downloaded from https://onlinelibrary.wiley.com/doi/10.1002/rnc.5394 by University Of Maryland, Wiley Online Library on [05/03/2024]. See the Terms and Conditions (https://onlinelibrary.wiley.com/terms-and-conditions) on Wiley Online Library for rules of use; OA articles are governed by the applicable Creative Commons License

where $B_{l_2}^{+}(t) = \hat{\Psi}^2(t)B_{l_2}^T(B_{l_2}\hat{\Psi}(t)B_{l_2}^T)^{-1}$. Notice that $B_{l_2}^{+}(t)$ is the weighted pseudoinverse of B_{l_2} since $B_{l_2}B_{l_2}^{+}(t) = I_{l_r}$ for all $\hat{\Psi}(t) \in \overline{\Psi}$. Moreover, when $\hat{\Psi}(t) = I$, then $B_{l_2}B_{l_2}^{+}(t) = B_{l_2}^T$. To examine the system stability during faults/failures, the norm boundedness of weighted pseudo-inverse of $B_{l_2}^{+}(t)$ is required. Specifically, a scalar ς_o exists that satisfies the following inequality as

$$\|B_{l_2}^{+}(t)\| = \|\hat{\Psi}^2(t)B_{l_2}^T(B_{l_2}\hat{\Psi}(t)B_{l_2}^T)^{-1}\| < \varsigma_o \tag{17}$$

for all $\hat{\psi}_i(t) \in \overline{\Psi}$ where $i = 1 \dots m_r$. Next, the virtual control input $\nu_r(t)$ associated with CA component in (12) is segregated as

$$\nu_r(t) = \nu_{r_l}(t) + \nu_{r_n}(t) \tag{18}$$

where $\nu_{r_l}(t) \in \mathfrak{R}^{l_r}$ is responsible for stabilization of Lipschitz nonlinear system, and $\nu_{r_n}(t) \in \mathfrak{R}^{l_r}$ is nonlinear term of virtual control law designed using adaptive-ISMC technique and is responsible to provide robustness against unknown external disturbance and uncertainty. Therefore, the rest of this article is focused on the design of virtual control law that satisfies the closed-loop stability condition. A detailed closed-loop stability analysis is performed to ensure the state trajectories converge to the sliding manifold in presence of faults/failures and fault estimation error.

2.2 | Design of nominal control law $\nu_{r_l}(t)$

The nominal part of virtual control law is now designed to stabilize the Lipschitz nonlinear system and to attain the desired performance. First, it is assumed that all the actuators are working normally and perfectly estimated, that is, ($\Delta(t) = 0$ & $\hat{\Psi}(t) = \Psi(t) = I_{m_r}$). The uncertain system (16), ignoring the effect of disturbance, is reduced to the following form

$$\dot{x}_r(t) = A_r x_r(t) + B_{\nu_r}\nu_{r_l}(t) + g_r(x_r, u_r, t) \tag{19}$$

where $B_{\nu_r} = B_{l_1} + B_\delta B_{l_2}^T$. Assuming (A_r, B_{ν_r}) is controllable, then the nominal control law is designed as

$$\nu_{r_l}(t) = -\mathcal{F}_r x_r(t) \tag{20}$$

where $\mathcal{F}_r \in \mathfrak{R}^{l_r \times n_r}$ is the state feedback gain and is designed to make the Lipschitz nonlinear system (19) stable.

Assumption 3. For a nonlinear system (19) with the control law (20), then there exists a unique equilibrium point x_{r_o} such that

$$0 = A_r x_{r_o} + B_{\nu_r}\mathcal{F}_r x_{r_o} + g_r(x_{r_o}, u_r, t). \tag{21}$$

Taking into account the Assumption 3, we define an error dynamics system $\tilde{x}_r(t) = x_r(t) - x_{r_o}$ and the time derivative after substituting (19-21) is obtained as

$$\dot{\tilde{x}}_r(t) = A_r\tilde{x}_r(t) - B_{\nu_r}\mathcal{F}_r\tilde{x}_r(t) + \tilde{g}_r \tag{22}$$

where $\tilde{g}_r = g_r(x_r, u_r, t) - g_r(x_{r_o}, u_r, t)$. The sufficient conditions are provided in the following theorem that ensured the stability of error dynamics (22).

Remark 5. In the nonlinear systems of the form (19) with a control law (20), there exists a multiple equilibrium points. In the existing work,[45] the author's assumed the strict inequality by assuming zero equilibrium point (i.e., $\|g_r(x_r, u_r, t)\| \leq \gamma_{x_r}x_r$). However, in the article, the stability results are obtained with non-zero equilibrium point x_{r_o}.

Theorem 1. *Consider a system (22) with the nominal state feedback control law (20), if the gain $\mathcal{F}_r$ is selected such that $\bar{A}_r = A_r - B_{\nu_r}\mathcal{F}_r$ is stable and*

$$\min_{\omega \in \mathfrak{R}^+} \sigma_{min}(\bar{A}_r - j\omega I) > \gamma_{x_r} \tag{23}$$

10991239, 2021, 6, Downloaded from https://onlinelibrary.wiley.com/doi/10.1002/rnc.5394 by University Of Maryland, Wiley Online Library on [05/03/2024]. See the Terms and Conditions (https://onlinelibrary.wiley.com/terms-and-conditions) on Wiley Online Library for rules of use; OA articles are governed by the applicable Creative Commons License

and there exists $\epsilon_1 > 0$ such that the following algebraic riccati equation (ARE)

$$\bar{A}_r^T P_r + P_r \bar{A}_r + \gamma_{x_r}^2 I + P_r P_r + \epsilon_1 I = 0 \tag{24}$$

has positive definite solution $P_r > 0 \in \mathfrak{R}^{n_r \times n_r}$, then the error dynamics (22) is asymptotic stable.

Proof. By following the results of Reference 30 (theorem 2), if condition (23) is satisfied, then there exists $\epsilon_1 > 0$ such that ARE in (24) has positive definite solution $P_r > 0$. Choose a Lyapunov function $V_r(t) = \frac{1}{2}\tilde{x}_r^T(t) P_r \tilde{x}_r(t)$, $P_r > 0$ and the time derivative of $V_r(t)$ after substituting (22) gives

$$\dot{V}_r(t) = \tilde{x}_r^T(\bar{A}_r^T P_r + P_r \bar{A}_r)\tilde{x}_r(t) + 2\tilde{x}_r^T(t) P_r \tilde{g}_r. \tag{25}$$

It is important to note that

$$\begin{aligned} 2\tilde{x}_r^T(t) P_r \tilde{g}_r &\leq 2\tilde{x}_r^T(t) P_r (g_r(x_r, u_r, t) - g_r(x_{r_o}, u_r, t)) \\ &\leq 2\gamma_{x_r} \|\tilde{x}_r^T(t) P_r\| \|\tilde{x}_r(t)\| \\ &\leq \gamma_{x_r}^2 \tilde{x}_r^T(t)\tilde{x}_r(t) + \tilde{x}_r^T(t) P_r P_r \tilde{x}_r(t). \end{aligned} \tag{26}$$

Using (26), $\dot{V}_r(t)$ becomes

$$\begin{aligned} \dot{V}_r(t) &= \tilde{x}_r^T(t)(\bar{A}_r^T P_r + P_r \bar{A}_r + \gamma_{x_r}^2 I + P_r P_r)\tilde{x}_r(t) \\ &< -\epsilon_1 \|\tilde{x}_r^T(t)\tilde{x}_r(t)\| \end{aligned} \tag{27}$$

which shows the asymptotic convergence of state variable $x_r(t)$ to the equilibrium point x_{r_o}. ∎

Remark 6. Theorem 1 provides the necessary condition for Lipschitz nonlinear system with Lipschitz constant γ_{x_r}. If the nonlinear system have multiple equilibrium point then Theorem 1 guarantees the convergence to each x_{r_o} according to the initial value of each state variable.

2.2.1 | State feedback synthesis

In this subsection, the stability condition of Theorem 1 is incorporated into synthesis framework in determining the state feedback gain $\mathcal{F}_r$. In this article, LQR formulation is adopted that synthesize the virtual control law $\nu_{r_l}(t)$ such that the feasible solution of the following LMI holds

$$\begin{bmatrix} A_r^T P_r + P_r A_r - Y_r^T B_{v_r}^T - B_{v_r} Y_r + \gamma_{x_r}^2 X_r X_r + I & (Q_{r_1} X_r - R_{r_1} Y_r)^T \\ (Q_{r_1} X_r - R_{r_1} Y_r) & -I \end{bmatrix} < 0 \tag{28}$$

where Q_{r_1} and R_{r_1} are the positive definite matrices that determine the nominal system performance, and X_r and Y_r are the decision variables. Once X_r and Y_r are synthesize state feedback gain is recovered as $\mathcal{F}_r = Y_r X_r^{-1}$.

Remark 7. In this article, a constraint is imposed while computing the gain $\mathcal{F}_r$ which determine the response of virtual nominal system. The LQR parameters Q_{r_1} and R_{r_1} are used to tune the system response according to the designer requirement.

2.3 | Design of adaptive-ISMC law

To develop the nonlinear adaptive-ISMC law, first define an integral type switching function as

$$\mathcal{S}_r(t) = \mathcal{H}_r(x_r(t) - x_r(0)) - \mathcal{H}_r \int_0^t (A_r - B_{v_r}\mathcal{F}_r)x_r(\tau) + g_r(x_r, u_r, \tau)d\tau \tag{29}$$

10991239, 2021, 6, Downloaded from https://onlinelibrary.wiley.com/doi/10.1002/rnc.5394 by University Of Maryland, Wiley Online Library on [05/03/2024]. See the Terms and Conditions (https://onlinelibrary.wiley.com/terms-and-conditions) on Wiley Online Library for rules of use; OA articles are governed by the applicable Creative Commons License

where $\mathcal{H}_r \in \mathfrak{R}^{l_r \times n_r}$ is a design freedom. The sliding motion is expected to occur on the sliding surface defined as

$$\gamma_r = \{x_r(t) \in \mathfrak{R}^{n_r} : S_r(t) = 0\}. \tag{30}$$

The time derivative of switching function (29) after substituting (16) becomes

$$\dot{S}_r(t) = \mathcal{H}_r \hat{B}_r(t) v_r(t) + \mathcal{H}_r D_r \Phi_r(x_r, t) + \mathcal{H}_r B_{v_r} \mathcal{F}_r x_r(t). \tag{31}$$

Next, the sliding dynamics is explored using the equivalent control method.[46] The equivalent control $\hat{v}_{r_{eq}}(t)$ is obtained by executing (31) to zero as

$$\hat{v}_{r_{eq}}(t) = (\mathcal{H}_r \hat{B}_r(t))^{-1}(-\mathcal{H}_r B_{v_r} \mathcal{F}_r x_r(t) - \mathcal{H}_r D_r \Phi_r(x_r, t)). \tag{32}$$

The equivalent control law (32) is substituted into (16) and the term $B_{v_r} \mathcal{F} x_r(t)$ is subtracted and added, then the corresponding sliding mode dynamics is achieved as

$$\begin{aligned} \dot{x}_r(t) = {} & (A_r - B_{v_r}\mathcal{F}_r)x_r(t) + g_r(x_r, u_r, t) + (B_{v_r} - \hat{B}_r(t)(\mathcal{H}_r \hat{B}_r(t))^{-1}\mathcal{H}_r B_{v_r})\mathcal{F}_r x_r(t) \\ & + \underbrace{(1 - \hat{B}_r(t)(\mathcal{H}_r \hat{B}_r(t))^{-1}\mathcal{H}_r)}_{\Lambda^*} D_r \Phi_r(x_r, t)) \end{aligned} \tag{33}$$

where Λ^* is treated as a unmatched term in the system. An appropriate choice of design freedom $\mathcal{H}_r$ can minimize the effect of mismatched term.[46] In this article, the design freedom matrix $\mathcal{H}_r$ is chosen as

$$\mathcal{H}_r = B_{l_2}(B_r^T B_r)^{-1} B_r^T. \tag{34}$$

With the choice of $\mathcal{H}_r$ in (34) and using the fact that $B_{l_2} B_{l_2}^T = I_{l_r}$, the following simplifications are made as

$$\begin{cases} \mathcal{H}_r B_{v_r} = B_{l_2}(B_r^T B_r)^{-1} B_r^T (B_{l_1} + B_\delta B_{l_2}^T) = B_{l_2}(B_r^T B_r)^{-1} B_r^T \underbrace{(B_{l_1} B_{l_2} + B_\delta)}_{B_r} B_{l_2}^T) = I_{l_r} \\ \mathcal{H}_r \hat{B}_p(t) = B_{l_2}(1 - \Delta(t) B_{l_2}^+(t)). \end{cases} \tag{35}$$

Remark 8. With the choice of $\mathcal{H}_r$ in (34) and based on proposition 3 in Reference 46, the matrix $\Lambda^* = (I - B_r(B_r^T B_r)^{-1} B_r^T)$ has Euclid norm equal to one (i.e., $\|\Lambda^*\| = 1$). Therefore, the resulting equivalent perturbation is equal to original unmatched perturbation $D_r \Phi_r(x_r, t)$, that is, $\|\Lambda^* D_r \Phi_r(x_r, t)\| \leq \|D_r \Phi_r(x_r, t)\|$.

Using $\mathcal{H}_r$ as defined in (34), the closed-loop uncertain system (33) can be simplified as

$$\dot{x}_r(t) = (A_r - B_{v_r}\mathcal{F}_r)x_r(t) + g_r(x_r, u_r, t) + D_r \Phi_r(x_r, t) + \tilde{B}_r \tilde{\phi}_r(t) \mathcal{F}_r x_r(t) \tag{36}$$

where $\tilde{B}_r = I_{n_r - l_r}$ and the unmatched term $\tilde{\phi}_r(t)$ is obtained as

$$\tilde{\phi}_r(t) = (B_{l_1} B_{l_2} + B_\delta)(B_{l_2}^T - (I_{m_r} - \Delta(t)) B_{l_2}^+ (B_{l_2}(I_{m_r} - \Delta(t)) B_{l_2}^+(t))^{-1}. \tag{37}$$

Remark 9. It is noticeable that in case of perfect estimation of actuator's effectiveness and when all the actuators are in healthy condition (i.e., $\hat{\Psi}(t) = I_{m_r}$), then matrix $B_{l_2}^+(t) = B_{l_2}^T|_{\hat{\Psi}(t)=I}$. Consequently, the uncertain term $\tilde{\phi}_r(t)$ in (37) is reduced to zero and the uncertain close-loop system (36) (neglecting the disturbance effect) is simplified to

$$\dot{x}_r(t) = A_r x_r(t) - B_{v_r}\mathcal{F}_r x_r(t) + g_r(x_r, u_r, t) \tag{38}$$

which is stable with the appropriate choice of $\mathcal{F}_r$. However, in the existence of the external disturbance/uncertainty and faults/failures, the terms $\Phi_r(x_r, t)$ and $\tilde{\phi}_r(t)$ become nonzero and are treated as unmatched uncertainty. Therefore, it is required to proof the stability of closed-loop uncertain system in the presence unmatched term.

10991239, 2021, 6, Downloaded from https://onlinelibrary.wiley.com/doi/10.1002/rnc.5394 by University Of Maryland, Wiley Online Library on [05/03/2024]. See the Terms and Conditions (https://onlinelibrary.wiley.com/terms-and-conditions) on Wiley Online Library for rules of use; OA articles are governed by the applicable Creative Commons License

2.3.1 | Analysis of closed-loop stability

In this subsection, the closed-loop stability analysis is performed using small gain theorem.[43] Using the Assumption 2, the closed-loop uncertain system in (36) can be written into the form as

$$\dot{x}_r(t) = \bar{A}_r x_r(t) + g_r(x_r, u_r, t) + \tilde{B}_r \tilde{u}_r(t) \tag{39}$$

$$\tilde{y}_r(t) = \tilde{\mathcal{F}}_a x_r(t) \tag{40}$$

$$\tilde{u}_r(t) = \tilde{\Xi}(t)\tilde{y}_r(t) \tag{41}$$

where $\bar{A}_r = A_r - B_{v_r}\mathcal{F}_r$, $\tilde{B}_r = \begin{bmatrix} I_{n_r - l_r} & I \end{bmatrix}$, $\tilde{\Xi}(t) = diag(\tilde{\phi}_r(t), \Phi_{r_{eq}}(t, x_r))$, and $\tilde{\mathcal{F}}_a = \begin{bmatrix} \mathcal{F}_r \\ I \end{bmatrix}$. To pursue further towards the stability analysis, define $\mathcal{L}_2$ norm from $\tilde{u}_r(t)$ to $\tilde{y}_r(t)$ as

$$\|\tilde{y}_r(t)\|^2_{\mathcal{L}_2} \leq \varsigma_2^2 \|\tilde{u}_r(t)\|^2_{\mathcal{L}_2}. \tag{42}$$

Since the system (39) is stable using the gain $\mathcal{F}_r$. Therefore, $\mathcal{L}_2$ norm is well defined.

Assumption 4. It is assumed that the augmented uncertainty satisfies the following inequality

$$\|\tilde{\Xi}_r(t)\| < \varsigma_a \quad \text{for all} \quad \hat{\Psi}(t) \in \overline{\Psi} \tag{43}$$

where ς_a is defined as an upper bound on the uncertain term.

Remark 10. Assumption 4 shows that the uncertainty term (43) is bounded. Since the faults, failures, and maximum estimation error are bounded (47)-(49), hence it is reasonable to impose the bound on uncertainty matrix.

Proposition 1. *For any combination of actuator's faults and failures pertaining to the set* $(\psi_1, ...\psi_{m_r}) \in \overline{\Psi}$ *, the uncertain closed-loop system (39)-(41) is stable if*

$$\varsigma_a \varsigma_2 < 1 \tag{44}$$

where ς_2 *is* $\mathcal{L}_2$ *norm from* $\tilde{u}_r(t)$ *to* $\tilde{y}_r(t)$ *and* ς_a *is defined in (43).*

Proof. The differential equation given in (39) can be seen as a negative feedback interconnection of Lipschitz nonlinear system (39) and the bounded uncertain term $\tilde{\Xi}_r(t)$. Based on the small gain theorem,[43] the closed-loop uncertain system (39)-(41) is stable subject to the faults/failures belonging to set $\overline{\Psi}$ if $\mathcal{L}_2$ norm from $\tilde{u}_r(t)$ to $\tilde{y}_r(t)$ satisfies the stability condition $\varsigma_2 < \frac{1}{\varsigma_a}$. To incorporate this condition, a bounded real lemma (BRL) formulation is used. The $\mathcal{L}_2$ norm from $\tilde{u}_r(t)$ to $\tilde{y}_r(t)$ is less than ς_2, if there exists Lyapunov function $V_r(t) = x_r^T(t) P_r x_r(t)$, $P_r > 0$ such that

$$\int_0^\infty \dot{V}_r(\tau) + \tilde{y}_r^T(\tau)\tilde{y}_r(\tau) - \varsigma_2^2 \tilde{u}_r^T(\tau)\tilde{u}_r(\tau) < 0 \tag{45}$$

holds for all $x_r(t)$ and $\tilde{u}_r(t)$.

To encapsulate the stability condition in (44), this is equivalent to finding the feasible solution of BRL[47]

$$\begin{bmatrix} A_r^T X_r + X_r A_r - B_{v_r} Y_r - Y_r^T B_{v_r}^T + \gamma_{x_r}^2 X_r X_r + I & \tilde{B}_r & Y_r^T \\ \tilde{B}_r^T & -\varsigma_2^2 I & 0 \\ Y_r & 0 & -I \end{bmatrix} < 0 \tag{46}$$

where $Y_r = \mathcal{F}_r X_r^{-1}$. Next it is required to proof the boundedness of uncertainty matrix $\Xi_r(t)$ to satisfy the Assumption 4. It can be seen that uncertain matrix is composed of two diagonal terms. The term associated with the disturbance input

10991239, 2021, 6, Downloaded from https://onlinelibrary.wiley.com/doi/10.1002/rnc.5394 by University Of Maryland, Wiley Online Library on [05/03/2024]. See the Terms and Conditions (https://onlinelibrary.wiley.com/terms-and-conditions) on Wiley Online Library for rules of use; OA articles are governed by the applicable Creative Commons License

$\Phi_{r_{eq}}(t, x_r)$ is assumed to be bounded (see Assumption 2) , where the uncertain term $\tilde{\phi}_r(t)$ depends on fault/failure and fault estimation error. To show $\tilde{\phi}_r(t)$ is bounded, (37) is written as

$$\|\tilde{\phi}_r(t)\| \leq (\|B_{l_1}B_{l_2}\| + \|B_\delta\|)\|(B_{l_2}^T - (1-\Delta(t))B_{l_2}^+(t))\|\|(B_{l_2}(1-\Delta(t))B_{l_2}^+(t))^{-1}\|. \tag{47}$$

Now using the fact, for a generic square matrix $\mathcal{Y}$, in general $\|(I-\mathcal{Y})^{-1}\| \leq (1-\|\mathcal{Y}\|)^{-1}$ if $\|\mathcal{Y}\| < 1$ and the fact $\|B_{l_2}\| = 1$ and $\|B_{l_2}B_{l_2}^+(t)\| = I_{l_r}$, (47) becomes

$$\|\tilde{\phi}_r(t)\| \leq (\|B_{l_1}\| + \|B_\delta\|)(1-(1+\Delta_{max})\|B_{l_2}^+(t)\|)(I - \|B_{l_2}\Delta(t)B_{l_2}^+(t)\|)^{-1}. \tag{48}$$

This is well defined $\|B_{l_2}\Delta(t)B_{l_2}^+(t)\| < \Delta_{max}\varsigma_o < 1$. Now define $\varsigma_1 = \|B_{l_1}\|$, $\varsigma_3 = \|B_\delta\|$ and $\|B_{l_2}^+(t)\| < \varsigma_o$ in (17), the inequality in (48) becomes

$$\|\tilde{\phi}_r(t)\| \leq \frac{(\varsigma_1+\varsigma_3)(1-(1+\Delta_{max})\varsigma_o}{1-\Delta_{max}\varsigma_o}. \tag{49}$$

Now the both diagonal terms in $\tilde{\Xi}(t)$ are bounded. Therefore, the augmented uncertainty term $\tilde{\Xi}(t)$ can satisfy the Assumption 4. It can now be concluded that if LMI given in (46) is feasible then the closed-loop system (39)-(41) is stable. This complete the proof. ∎

Remark 11. The choice of state feedback gain has a significant impact on the stability of overall system (39)-(41). Therefore, in this article, we imposed two constraints on the design of feedback gain $\mathcal{F}_r$ and both are required to satisfy simultaneously to ensure the closed-loop stability and fulfillment of desired performance. On the other hand, the estimation error Δ_{max} in (49) also impact on the norm of uncertainty term given in (43). Therefore, with the good estimation, the less stringent requirement on $\mathcal{L}_2$ norm from $\tilde{u}_r(t)$ to $\tilde{y}_r(t)$ given in (42).

In the SMC literature, the reachability condition is required to be satisfied. Therefore in the upcoming subsection, the control law is designed that ensures the sliding motion onto the sliding surface.

2.3.2 | Design of $\nu_{r_n}(t)$

An adaptive nonlinear ISMC component $\nu_{f_n}(t)$ is defined as

$$\nu_{r_n}(t) = -\Gamma_r(x_r, t)\frac{\mathcal{S}_r(t)}{\|\mathcal{S}_r(t)\|} \tag{50}$$

where $\Gamma_r(x_r, t)$ is defined as the modulation gain and is updated according to the following law.

- If $\|\mathcal{S}_r(t)\| > \epsilon$ where ϵ is a small threshold value, then $\Gamma_r(x_r, t)$ is updated according to the following law

$$\Gamma_r(x_r, t) = \overline{\Gamma}\int_0^t \|\mathcal{S}_r(\tau)\|d\tau \tag{51}$$

  where $\overline{\Gamma} > 0$ and $\Gamma_r(0) > 0$
- If $\|\mathcal{S}_r(t)\| \leq \epsilon$, then $\Gamma_r(x_r, t)$ is read as

$$\begin{aligned}\Gamma_r(x_r, t) &= \overline{\Gamma}_2\|\eta\| + \overline{\Gamma}_3\\ \tau\dot{\eta} + \eta &= sign(\mathcal{S}_r(t))\end{aligned} \tag{52}$$

  where $\overline{\Gamma}_2 = \Gamma_r(t^*)$, $\overline{\Gamma}_3 > 0$ and $\tau > 0$.

When $\|\mathcal{S}_r(t)\| > \epsilon$, Γ_r is updated according to the law (51) to counteract the effect of disturbance/uncertainty occurs due to faults and failures till the sliding starts, say that the time t_1. When the sliding has started, that is, $\|\mathcal{S}_r(t)\| < \epsilon$ &

10991239, 2021, 6, Downloaded from https://onlinelibrary.wiley.com/doi/10.1002/rnc.5394 by University Of Maryland, Wiley Online Library on [05/03/2024]. See the Terms and Conditions (https://onlinelibrary.wiley.com/terms-and-conditions) on Wiley Online Library for rules of use; OA articles are governed by the applicable Creative Commons License

$t > t_1$, the gain Γ_r is updated according to the law (52). Thus the adaptive law (52) allows the gain to adjust to the lower value to counteract the current disturbance/uncertainty.

Remark 12. The adaptive law (51)-(52) differs from the existing methods proposed in References 41 and 42. In References 41 and 42, the adaptive gain rises until the sliding motion reaches the zero sliding surface. The larger gain causes the undesirable chattering effect and it is practically not possible to achieve the zero sliding surface. In this article, the proposed adaptive strategy (51)-(52) raises the adaptive gain only when the sliding motion exceeds the threshold value of ϵ. In this way, the chattering effect can be reduced significantly.[60]

Proposition 2. *For an uncertain system (16), with the sliding surface (29) controlled by the ISMC law (50), then there exists an maximum upper bound Γ_r^* such that*

$$\|\Gamma_r(x_r, t)\| \leq \Gamma_r^* \tag{53}$$

where Γ_r^* is the maximum modulation gain and is generally chosen higher than disturbance/uncertainty norms in the system. In our case, it can be selected as

$$\Gamma_r^* \geq \frac{\Delta_{max}\varsigma_o\|v_{f_l}\| + \|\mathcal{H}_r\Phi_r(x_r, t)\|}{1 - \Delta_{max}\varsigma_o} \tag{54}$$

Proof. See the Appendix. ∎

Theorem 2. *Given the uncertain system (16), the virtual control law (18) along with ISMC component (50) will maintain the sliding during faults/failures, if the modulation gain $\Gamma_r(x_r, t)$ is updated according to the adaption law (51)-(52).*

Proof. The proof of theorem is done in two steps ∎

- Consider first $\|\mathcal{S}_r(t)\| > \epsilon$, then the modulation gain $\Gamma_r(x_r, t)$ is updated according to (51). Define the Lyapunov function as

$$V_r(t) = \frac{1}{2}\mathcal{S}_r^T(t)\mathcal{S}_r(t) + \frac{1}{2\mu}(\Gamma_r(x_r, t) - \Gamma_r^*)^2. \tag{55}$$

The time derivative of $V_r(t)$ after substituting (18), (31), (35), and (50)-(51) becomes

$$\begin{aligned}
\dot{V}_r(t) &= \mathcal{S}_r^T(t)(-\Gamma_r(x_r, t)\frac{\mathcal{S}_r(t)}{\|\mathcal{S}_r(t)\|} + \mathcal{H}_r\Phi_r(x_r, t) + B_{l_2}\Delta(t)B_{l_2}^+(t)(\mathcal{F}_r x_r(t) \\
&\quad + \Gamma_r\frac{\mathcal{S}_r(t)}{\|\mathcal{S}_r(t)\|})) + \frac{1}{\mu}(\Gamma_r - \Gamma_r^*)\overline{\Gamma}\|\mathcal{S}_r(t)\| \\
&\leq \|\mathcal{S}_r(t)\|\left(-\Gamma_r + \|\mathcal{H}_r\Phi_r(x_r, t)\| + \Delta_{max}\varsigma_o(\|v_{f_l}(t)\| + \Gamma_r)\right) + \frac{1}{\mu}(\Gamma_r - \Gamma_r^*)\overline{\Gamma}\|\mathcal{S}_r(t)\| \\
&= \underbrace{\Delta_{max}\varsigma_o\|v_{f_l}\| + \|\mathcal{H}_r\Phi_r(x_r, t)\|}_{\Psi_M}\|\mathcal{S}_r(t)\| - \Gamma_r\underbrace{(1 - \Delta_{max}\varsigma_o)}_{\lambda_M}\|\mathcal{S}_r(t)\| + \lambda_M\Gamma_r^*\|\mathcal{S}_r(t)\| \\
&\quad - \lambda_M\Gamma_r^*\|\mathcal{S}_r(t)\| + \frac{1}{\mu}(\Gamma_r - \Gamma_r^*)\overline{\Gamma}\|\mathcal{S}_r(t)\| \\
&= (\Psi_M - \lambda_M\Gamma_r^*)\|\mathcal{S}_r(t)\| + (\Gamma_r - \Gamma_r^*)(-\lambda_M\|\mathcal{S}_r(t)\| + \frac{1}{\mu}\overline{\Gamma}\|\mathcal{S}_r(t)\|).
\end{aligned} \tag{56}$$

It follows from proposition 2, there exists Γ_r^* such that $\|\Gamma_r - \Gamma_r^*\| < 0$ for all $t > 0$. It yields

$$\dot{V}_r(t) = -\underbrace{(-\Psi_M + \lambda_M\Gamma_r^*)}_{\alpha_M}\|\mathcal{S}_r(t)\| - \|\Gamma_r - \Gamma_r^*\|\underbrace{(-\lambda_M\|\mathcal{S}_r(t)\| + \frac{1}{\mu}\overline{\Gamma}\|\mathcal{S}_r(t)\|)}_{\beta_M}. \tag{57}$$

10991239, 2021, 6, Downloaded from https://onlinelibrary.wiley.com/doi/10.1002/rnc.5394 by University Of Maryland, Wiley Online Library on [05/03/2024]. See the Terms and Conditions (https://onlinelibrary.wiley.com/terms-and-conditions) on Wiley Online Library for rules of use; OA articles are governed by the applicable Creative Commons License

FIGURE 2 Octorotor configuration[53]

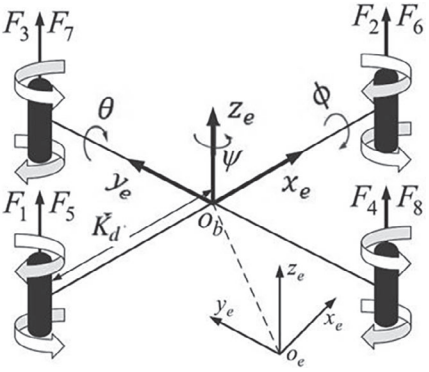

There exist $\Gamma_r^* > \frac{\Psi_M}{\lambda_M}$ and $\mu < \frac{\bar{\Gamma}}{\lambda_M}$ which yields $\alpha_M, \beta_M > 0$. One can get

$$\begin{aligned}\dot{V}_r(t) &= -\alpha_M\sqrt{2}\frac{\|S_r(t)\|}{\sqrt{2}} - \beta_M\sqrt{2\mu}\frac{\|\Gamma_r - \Gamma_r^*\|}{\sqrt{2\mu}} \\ &\leq -min(\alpha_M\sqrt{2} + \beta_M\sqrt{2\mu})\left(\frac{\|S_r(t)\|}{\sqrt{2}} - \frac{\|\Gamma_r - \Gamma_r^*\|}{\sqrt{2\mu}}\right) \leq -\gamma\sqrt{V_r}\end{aligned} \tag{58}$$

where $\gamma = min(\alpha_M\sqrt{2} + \beta_M\sqrt{2\mu})$. Therefore, convergence toward the sliding manifold is guaranteed in finite time.

- Now it is supposed that $\|S_r(t)\| \leq \epsilon$, then as claimed in Reference 48 (theorem 1), if Γ_r is larger enough with respect to disturbance/uncertainty in the system, then ISMC law (50) together with the adaptive law (52) allows keeping the system trajectories (1) to remain on the sliding surface $\|S_r\| < \epsilon$. Given the trajectories of system (16) reach $\|S_r(t)\| < \epsilon$, then it means that Γ_r is larger enough as per the theorem 1 of Reference 48. Thus the sliding is established for all $t > t_r$.

Finally, the total control effort $u_r(t)$ is extracted by gathering (12), (13), (18), (20), and (50) as

$$u_r(t) = -\hat{\Psi}(t)B_{l_2}^T(B_{l_2}\hat{\Psi}(t)B_{l_2}^T)^{-1}\left(\mathcal{F}_r x_r(t) + \Gamma_r(x_r,t)\frac{S_r(t)}{\|S_r(t)\|}\right) \quad \text{for} \quad S_r(t) \neq 0. \tag{59}$$

3 | APPLICATION OF NONLINEAR COAXIAL OCTOROTOR SYSTEM

The FTC scheme is tested on the Lipschitz nonlinear model of octorotor UAV. Because the octorotor UAV has better FTC capability and can even handle the total failure of primary rotors (four rotors) compared to quadrotor[49] and hexarotor[50] UAVs. Two types of octorotor configurations are used in the existing literature, the first one is star-shaped configuration given in References 51 and 52 and the other is the co-axial configuration recent proposed in References 53 and 54. The co-axial configuration offers several advantages over star-shaped in terms of stability, size, and higher thrust to weight ratio. The coaxial octorotor configuration is shown in Figure 2.

The nonlinear dynamics of the octorotor UAV are derived based on the following assumptions

1. The origin of body-fixed frame coincides with the center of mass (COM) of the octorotor UAV.
2. The axes of the body-fixed frame are coincident with the principal axes of inertia of the octorotor helicopter.

These assumptions are quite common in the existing work.[53,54] The benefits of these assumptions include the inertial matrix becomes diagonal and there is no requirement to take another COM. The forces acting on the octorotor system is obtained by combining gravitation force, thrust force, and translational motion including drag force which is described by the following differential equations[54]

$$\begin{bmatrix}\ddot{x}_e \\ \ddot{y}_e \\ \ddot{z}_e\end{bmatrix} = \begin{bmatrix}0 \\ 0 \\ g\end{bmatrix} + \frac{1}{m}\begin{bmatrix}(C_\phi C_\theta C_\psi + S_\phi S_\psi)u_z \\ (C_\phi C_\theta C_\psi - S_\phi S_\psi)u_z \\ C_\phi C_\theta u_z\end{bmatrix} + \frac{1}{m}\begin{bmatrix}K_x\dot{x}_e \\ K_y\dot{y}_e \\ K_z\dot{z}_e\end{bmatrix} \tag{60}$$

10991239, 2021, 6, Downloaded from https://onlinelibrary.wiley.com/doi/10.1002/rnc.5394 by University Of Maryland, Wiley Online Library on [05/03/2024]. See the Terms and Conditions (https://onlinelibrary.wiley.com/terms-and-conditions) on Wiley Online Library for rules of use; OA articles are governed by the applicable Creative Commons License

where $S_{(.)}$, $C_{(.)}$, and $T_{(.)}$ represent the trigonometric function $sin(.)$, $cos(.)$, and $tan(.)$, and x_e, y_e and z_e represent the position of vehicle in body-fixed frame, ϕ, θ, and ψ denote the roll angle, pitch angle, and yaw angles with respect to inertial frame of reference, m defines the vehicle mass, g shows the gravity, K_x, K_y, and K_z denote the drag coefficients and u_z is the total thrust generated by the motors. Similarly, the moment equations are obtained by combining gyroscopic torque, torque generated by motor, and induced torque obtained by rotational motion as

$$\begin{bmatrix} \dot{p} \\ \dot{q} \\ \dot{r} \end{bmatrix} = I^{-1}\left(-\begin{bmatrix} 0 & I_z r & -I_y q \\ I_z r & 0 & I_z p \\ I_y q & -I_z p & 0 \end{bmatrix}\begin{bmatrix} p \\ q \\ r \end{bmatrix} + I_r \begin{bmatrix} -q \\ p \\ 0 \end{bmatrix}\Omega + \begin{bmatrix} u_\phi \\ u_\theta \\ u_\psi \end{bmatrix} + \begin{bmatrix} -K_p K_d \dot{\phi} \\ -K_q K_d \dot{\theta} \\ -K_r K_d \dot{\psi} \end{bmatrix}\right) \tag{61}$$

where I denotes the inertial matrix define as $I = diag(I_x, I_y, I_z)$, p, q, and r are the vehicle rotational velocity with respect to the body-fixed frame, I_r is the rotor inertial moment, K_d is the distance between motor and COM of vehicle, K_p, K_q, and K_r are the drag coefficients, u_ϕ, u_θ, and u_ψ are the roll input, pitch input, and yawing moment to the system, and Ω is the residual speed of individual propeller defined as[54]

$$\Omega = \Omega_1 + \Omega_2 + \Omega_7 + \Omega_8 - \Omega_3 - \Omega_4 - \Omega_5 - \Omega_6 \tag{62}$$

where $\Omega_1 \ldots\ldots \Omega_8$ are the rotors speed. The angular velocity with respect to Earth fixed frame is obtained by performing the following multiplication

$$\begin{bmatrix} \dot{\phi} \\ \dot{\theta} \\ \dot{\psi} \end{bmatrix} = \begin{bmatrix} 1 & T_\theta S_\phi & T_\theta C_\phi \\ 0 & C_\phi & -S_\phi \\ 0 & \frac{S_\phi}{C_\theta} & \frac{C_\phi}{C_\theta} \end{bmatrix}\begin{bmatrix} p \\ q \\ r \end{bmatrix}. \tag{63}$$

The relationship between the control input to the system u_z, u_ϕ, u_θ, and u_ψ and the thrust generated by each motor is given by the following relationship[54]

$$\begin{bmatrix} u_z \\ u_\phi \\ u_\theta \\ u_\psi \end{bmatrix} = \underbrace{\begin{bmatrix} 1 & 1 & 1 & 1 & 1 & 1 & 1 & 1 \\ -l\frac{\sqrt{2}}{2} & -l\frac{\sqrt{2}}{2} & -l\frac{\sqrt{2}}{2} & -l\frac{\sqrt{2}}{2} & l\frac{\sqrt{2}}{2} & l\frac{\sqrt{2}}{2} & l\frac{\sqrt{2}}{2} & l\frac{\sqrt{2}}{2} \\ -l\frac{\sqrt{2}}{2} & -l\frac{\sqrt{2}}{2} & l\frac{\sqrt{2}}{2} & l\frac{\sqrt{2}}{2} & l\frac{\sqrt{2}}{2} & l\frac{\sqrt{2}}{2} & -l\frac{\sqrt{2}}{2} & -l\frac{\sqrt{2}}{2} \\ -\frac{d}{b} & \frac{d}{b} & \frac{d}{b} & -\frac{d}{b} & -\frac{d}{b} & \frac{d}{b} & \frac{d}{b} & -\frac{d}{b} \end{bmatrix}}_{B_{r_2}}\begin{bmatrix} F_1 \\ . \\ . \\ F_8 \end{bmatrix} \tag{64}$$

where $F_i = b\Omega_i^2$ is the thrust developed by individual rotor, b denotes the lift coefficient, l represents the moment arm length, d denotes drag force, respectively.

3.1 | Actuator dynamics

In this article, the dynamics of the actuator (driving motors) are considered in nonlinear simulations and are represented as first-order lag[53]

$$F_i = b\frac{\omega_i}{s + \omega_i}u_{a_i} \tag{65}$$

where ω_i shows the bandwidth of actuator, F_i is the actual thrust/force developed by ith rotor and u_{a_i} is pulse-width-modulation signal input to the motor. It is noticeable that the desired thrust, required by the controller, is provided by the corresponding actuator model.

10991239, 2021, 6, Downloaded from https://onlinelibrary.wiley.com/doi/10.1002/rnc.5394 by University Of Maryland, Wiley Online Library on [05/03/2024]. See the Terms and Conditions (https://onlinelibrary.wiley.com/terms-and-conditions) on Wiley Online Library for rules of use; OA articles are governed by the applicable Creative Commons License

TABLE 1 Variation in Plant parameters

Parameters	Case 1 (5% Uncertainty)	Case 2 (10% Uncertainty)	Case 3 (15% uncertainty)
I_x	4.62×10^{-2} Kg.m^2	4.84×10^{-2} Kg.m^2	5.06×10^{-2} Kg.m^2
I_y	4.62×10^{-2} Kg.m^2	4.84×10^{-2} Kg.m^2	5.06×10^{-2} Kg.m^2
I_z	9.24×10^{-2} Kg.m^2	9.68×10^{-2} Kg.m^2	10.02×10^{-2} Kg.m^2
b	1.05×10^{-6} N.s^2	1.1×10^{-6} N.s^2	1.15×10^{-6} N.s^2
d	0.315×10^{-6} m.s^2	0.33×10^{-6} m.s^2	0.345×10^{-6} m.s^2
l	0.42 m	0.44 m	0.46 m
m	1.575 Kg	1.65 Kg	1.725 Kg

3.2 | A benchmark wind model: Dryden turbulence model

In this work, the wind- gust effect is considered in nonlinear simulations. A Dryden wind model, given in Reference 55, is used to represent the wind-gust condition. The Dryden wind model is available as a built-in function in MATLAB that implements the mathematical representation given in Military Handbook MIL-HDBK-1797B.[56] The mean wind speed of 3 m/s and direction 240° at 6 m are given at the input of the Dryden turbulence model. The wind direction is measured from the North in a clockwise positive setting. The model output is the gust velocity at the body-fixed frame.

3.3 | Sensor noise and parameter uncertainties

In this article, the sensor noise and parameter uncertainties are also included in the nonlinear model to inpect robustness feature. A sensor noise is represented as band-limited white noise of variance 1×10^{-3} that is added to states $\dot{z}_e, p, q$, and r. To consider the parameter uncertainties, three different levels of uncertainties (5%, 10%, and 15%) are added to the original model parameters. The value of parameters that are considered in the nonlinear simulations is given in Table 1.

3.4 | Model decomposition

It is observed from nonlinear model (60)-(63) that the angles and their time derivatives are not relying of translational components, whereas the translational components (x_e, y_e, and z_e) are effected by the rotational axis. Therefore, the overall control strategy is segregated into two loops: the inner-loop and the outer-loop. The proposed FTC scheme is applied to inner-loop subsystem that contains the states vector $x_r(t) = \{z_e, \phi, \theta, \psi, \dot{z}_e, p, q, r\}$ whereas in outer-loop, nonlinear dynamics inversion (NDI) based SMC is proposed to achieve desired translation tracking of the states $x_s(t) = \{x_e, y_e, \dot{x}_e, \dot{y}_e\}$ and as well as provide desired roll ϕ_d and pitch commands θ_d. NDI technique is chosen for outer-loop to handle the nonlinear dynamics and coupling effect in the system. However, the robustness to baseline NDI controller is provided by SMC law. The outer-loop belongs to the internal dynamics of system. Therefore to ensure the stability of whole system, the internal dynamics are required to be stable.

Assumption 5. Assuming the perturbation from hovering is small, that is, $\{(\dot{\phi}, \dot{\theta}, \dot{\psi}) \cong (p, q, r)\}$.

This assumption is quite common in the existing literature.[51-54] Based on Assumption 5, the nonlinear equation of motion (60)-(63) associated with inner-loop subsystem $x_r(t)$ is converted into Lipschitz nonlinear form defined as

$$\underbrace{\begin{bmatrix} \dot{x}_{r_1}(t) \\ \dot{x}_{r_2}(t) \end{bmatrix}}_{\dot{x}_r(t)} = \underbrace{\begin{bmatrix} 0_{4\times4} & I_4 \\ 0_{4\times4} & 0_{4\times4} \end{bmatrix}}_{A_r} \underbrace{\begin{bmatrix} x_{r_1}(t) \\ x_{r_2}(t) \end{bmatrix}}_{x_r(t)} + \underbrace{\begin{bmatrix} 0_{4\times4} \\ B_{r_1} \end{bmatrix}}_{B_r} B_{r_2} u_r(t) + \underbrace{\begin{bmatrix} 0_{4\times4} \\ D_{r_1} \end{bmatrix}}_{D_r} \Phi_r(x_r, t) + \underbrace{\begin{bmatrix} 0_{4\times4} \\ g_{r_1}(x_r, u_r, t) \end{bmatrix}}_{g_r x_r, u_r, t} \tag{66}$$

10991239, 2021, 6, Downloaded from https://onlinelibrary.wiley.com/doi/10.1002/rnc.5394 by University Of Maryland, Wiley Online Library on [05/03/2024]. See the Terms and Conditions (https://onlinelibrary.wiley.com/terms-and-conditions) on Wiley Online Library for rules of use; OA articles are governed by the applicable Creative Commons License

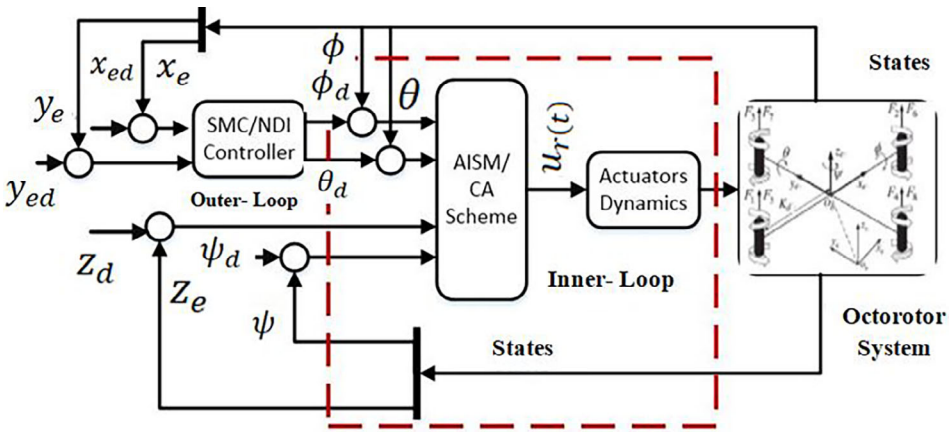

FIGURE 3 Architecture of controller implementation to octorotor system [Colour figure can be viewed at wileyonlinelibrary.com]

TABLE 2 Parameters of octorotor system

$I_x = 4.4\times10^{-2}$ Kg.m^2	$I_y = 4.4\times10^{-2}$ Kg.m^2	$I_z = 8.8\times10^{-2}$ Kg.m^2
$b = 1\times10^{-6}$ N.s^2	$I_r = 9\times10^{-5}$	$m = 1.5$ Kg
$g = 9.8$m/s^2	$l = 0.4$ m	$d = 0.3\times10^{-6}$m.s^2
$b = 1\times10^{-5}$N.s^2	$K_p, K_q, K_r = 0.01$	$K_x, K_y, K_z = 0.01$

where $x_{r_1}(t) = \{\phi, \theta, \psi, z_e\}, x_{r_2}(t) = \{\dot{z}_e, p, q, r\}$, $B_{r_1} = diag(r_1, r_4, r_7, r_9)$, $g_{r_1}(x_r, u_r, t) = col(r_1(C_\phi C_\theta - 1), r_2 qr, r_5 pr.r_8 pq)$, $\Phi_r(x_r, t) = col(\dot{z}_e, p, q, r)$, and $D_{r_1} = \begin{bmatrix} K_z/m & 0 & 0 & 0 \\ 0 & -K_pK_d & -r_3 & 0 \\ 0 & r_6 & -K_pK_d & 0 \\ 0 & 0 & 0 & -K_rK_d \end{bmatrix}$ whereas $r_1 = \frac{1}{m}, r_2 = \frac{I_y - I_z}{I_x}, r_3 = \frac{J_r}{I_x}\Omega, r_4 = \frac{1}{I_x}, r_5 = \frac{I_z - I_x}{I_y}, r_6 = \frac{J_r}{I_y}\Omega, r_7 = \frac{1}{I_y}, r_8 = \frac{I_x - I_y}{I_z}, r_9 = \frac{1}{I_z}$. To generate required roll ϕ_d reference and pitch θ_d reference to the inner-loop, the nonlinear dynamics of position subsystem (60) are linearized as[57]

$$\underbrace{\begin{bmatrix} \ddot{x}_e \\ \ddot{y}_e \end{bmatrix}}_{\ddot{x}_s} = \underbrace{\begin{bmatrix} C_\psi S_\phi - S_\phi S_\theta S_\psi \\ -S_\psi S_\phi - C_\phi S_\theta C_\psi \end{bmatrix} \frac{u_z}{m}}_{f_s(x_r)} - \underbrace{\frac{u_z}{m} \begin{bmatrix} C_\psi C_\phi + S_\phi S_\theta S_\psi & -C_\phi C_\theta S_\psi \\ -S_\psi C_\phi + S_\phi S_\theta C_\psi & -C_\psi C_\theta C_\phi \end{bmatrix}}_{g_s(x_r)} \underbrace{\begin{bmatrix} \Delta\phi_d \\ \Delta\theta_d \end{bmatrix}}_{u_s(t)} + \underbrace{\begin{bmatrix} \frac{K_x}{m} & 0 \\ 0 & \frac{K_y}{m} \end{bmatrix}}_{D_s} \underbrace{\begin{bmatrix} \dot{x}_e \\ \dot{y}_e \end{bmatrix}}_{\Phi_s(x_s,t)} \quad (67)$$

where $\Delta\phi_d = \phi_d - \phi$ and $\Delta\theta_d = \theta_d - \theta$, $\Delta\phi_d$ and $\Delta\theta_d$ denote the correction in roll and pitch commands. The designed FTC strategy is utilized to attain control of inner-loop subsystem given in (66), whereas NDI based SMC is designed for an outerloop subsystem that generates necessary ϕ_d and θ_d to inner-loop subsystem. The block diagrams of overall controller implementation is provided in Figure 3.

4 | IMPLEMENTATION OF FTC SCHEME TO OCTOROTOR UAV

4.1 | Control parameters settings

The proposed adaptive-ISMC based CA scheme is applied to Lipschitz nonlinear model of aircraft (66). The model parameters, used in the simulation, are given in Table 2. For an inner-loop state vector x_r, the control variables are z_e, ϕ, θ and ψ. Therefore choose $l_r = 4$.

The input distribution matrix B_r, defined in (66) is segregated into the form (7), where B_{l_1} and B_{l_2} are obtained as

$$B_{l_1} = \begin{bmatrix} 0 & 0 & 0 & 0 \\ 0 & 0 & 0 & 0 \\ 0 & 0 & 0 & 0 \\ 0 & 0 & 0 & 0 \\ 0 & 0 & 0 & -2.2 \\ -20.1 & 20.1 & 0 & 0 \\ 20.1 & 20.1 & 0 & 0 \\ 0 & 0 & 26.1 & 0 \end{bmatrix}, B_{l_2} = \begin{bmatrix} 0 & 0.5 & 0 & -0.5 & 0 & 0.5 & 0 & -0.5 \\ -0.5 & 0 & 0.5 & 0 & -0.5 & 0 & 0.5 & 0 \\ -0.3536 & -0.3536 & -0.3536 & -0.3536 & 0.3536 & 0.3536 & 0.3536 & 0.3536 \\ -0.3536 & -0.3536 & -0.3536 & -0.3536 & -0.3536 & -0.3536 & -0.3536 & -0.3536 \end{bmatrix}$$

10991239, 2021, 6, Downloaded from https://onlinelibrary.wiley.com/doi/10.1002/rnc.5394 by University Of Maryland, Wiley Online Library on [05/03/2024]. See the Terms and Conditions (https://onlinelibrary.wiley.com/terms-and-conditions) on Wiley Online Library for rules of use; OA articles are governed by the applicable Creative Commons License

where B_δ can be computed using (7). Next, it can be verified that $\varsigma_1 = \|B_{l_1}\| = 0.658$ and $\varsigma_3 = \|B_\delta\| = 0.11$ and $B_{l_2}B_{l_2}^T = I_{l_r}$. The Lipschitz constants in (2) are obtained as $\gamma_{x_r} = 0.67$. The LQR parameters are chosen as $Q_{r_1} = diag(10, 10, 10, 10, 1, 1, 1, 1)$ and $R_{r_1} = diag(0.1, 0.2, 0.5, 1)$. Based on the LQR parameters, LMI given in (28) and (46) are solved using LMI toolbox in MATLAB and optimal value of feedback gain $\mathcal{F}_r$ is obtained as

$$\mathcal{F}_r = \begin{bmatrix} 0 & -7.0711 & 7.0711 & 0 & 0 & -0.5941 & 0.5941 & 0 \\ 0 & 5 & 5 & 0 & 0 & 0.4996 & 0.4996 & 0 \\ 0 & 0 & 0 & 4.4721 & 0 & 0 & 0 & 0.5858 \\ -3.1623 & 0 & 0 & 0 & -1.7050 & 0 & 0 & 0 \end{bmatrix}. \tag{68}$$

Using Equation (42), the computed gain $\varsigma_2 = 0.3213$, therefore, the maximum bound on uncertain term (43) should be less than 1/0.3213 to satisfy the stability condition given in (44). The parameters of adaptive modulation gain (51)-(52) are selected, in light of several nonlinear simulations, as $\Gamma_r(0) = 5$, $\overline{\Gamma} = 100$, $\overline{\Gamma}_2 = 4.5, \overline{\Gamma}_3 = 5$, $\tau = 0.1$, $\mu = 0.1, \epsilon = 2 \times 10^{-4}$. The motor bandwidth in (65) is chosen as $\omega_i = 20 rad/s$.

4.2 | Estimation of actuator effectiveness $\hat{\Psi}(t)$

In this article, the actuator effectiveness $\hat{\Psi}(t)$ is estimated using adaptive SMO (ASMO) based fault estimation scheme proposed in Reference 41. It is well known that the any fault or failure in the system during hovering and vertical take off mode can cause catastrophic consequences which can leads to the crash.[58] Therefore we take a linearized model of octorotor UAV at vertical take off position instead of complex nonlinear model. To implement ASMO to octorotor UAV, the nonlinear system is linearized at vertical take off position (i.e., $(\dot{\phi}, \dot{\theta}, \dot{\psi}) \approx 0$) and the nonlinear system (66) can be written as

$$\begin{aligned} \dot{x}_r(t) &= A_r x_r(t) + B_r \Psi(t) u_r(t) + D_r \Phi_r(x_r, t) \\ y_r(t) &= C_r x_r(t) \end{aligned} \tag{69}$$

where the parameters A_r, B_r are the same as defined in (66), $C_r = [I_4 \ 0_{4\times 4}] \in \Re^{4\times 8}$, and in new setting $D_r = K_z/m$ and $\Phi_r(x_r, t) = \dot{z}_e$. The ASMO for the system (69) is defined a

$$\dot{\hat{x}}_r(t) = A_r \hat{x}_r(t) + B_r \hat{\Psi}(t) u_r(t) + \mathcal{L}_r C_r \tilde{x}_r(t) + D_r \nu_{r_e}(t) \tag{70}$$

where $\tilde{x}_r(t) = x_r(t) - \hat{x}_r(t)$, $\mathcal{L}_r \in \Re^{8\times 4}$ is the observer gain matrix and is computed to make the system $A_r - \mathcal{L}_r C_r$ Hurwitz and $\nu_{r_e}(t)$ is the nonlinear injection term defined as

$$\nu_{r_e}(t) = -\Gamma_e \frac{\tilde{x}_r(t)}{\tilde{x}_r(t)}, \quad \tilde{x}_r(t) \neq 0. \tag{71}$$

Γ_e is the modulation gain chosen as $\Gamma_e \geq \|\Phi_r(x_r, t)\|$. The error dynamic equation is defined as

$$\dot{\tilde{x}}_r(t) = A_r \tilde{x}_r(t) + \mathcal{L}_r C_r \tilde{x}_r(t) + \sum_{j=1}^{8} b_{r_i} \tilde{\psi}_i(t) u_{r_i}(t) \tag{72}$$

where $\tilde{\psi}_i(t) = \psi_i(t) - \hat{\psi}(t)$ and $\hat{\psi}_i(t)$ is updated as

$$\dot{\hat{\psi}}(t) = Proj \begin{cases} 0 & if \quad \hat{\psi}(t) = \psi_{min}, l_{r_i} \tilde{x}_r^T \mathcal{P} b_{r_i} u_{r_i}(t) \leq 0 \\ l_{r_i} \tilde{x}_r^T \mathcal{P} b_{r_i} u_{r_i}(t) & \text{otherwise} \end{cases} \tag{73}$$

where *Proj* define as projection operator, l_{r_i} determines the adaption speed and is chosen as $l_{r_i} = 2$, the observer gain $\mathcal{L}_r$ and symmetric positive definite matrix $\mathcal{P}$ are obtained by solving inequality given in Reference 41 (see (43) in Reference 41) as

10991239, 2021, 6, Downloaded from https://onlinelibrary.wiley.com/doi/10.1002/rnc.5394 by University Of Maryland, Wiley Online Library on [05/03/2024]. See the Terms and Conditions (https://onlinelibrary.wiley.com/terms-and-conditions) on Wiley Online Library for rules of use; OA articles are governed by the applicable Creative Commons License

$$\mathcal{L}_r = \begin{bmatrix} 5.6 & 0 & 0 & 0 & 7.77 & 0 & 0 & 0 \\ 0 & 8.8 & 0 & 0 & 0 & 18.72 & 0 & 0 \\ 0 & 0 & 3.6 & 0 & 0 & 0 & 3.15 & 0 \\ 0 & 0 & 0 & 3.7 & 0 & 0 & 0 & 3.2 \end{bmatrix}^T, \quad \mathcal{P} = \begin{bmatrix} 2.7 & 0 & 0 & 0 & 2.5 & 0 & 0 & 0 \\ 0 & 2.9 & 0 & 0 & 0 & 2.7 & 0 & 0 \\ 0 & 0 & 3.2 & 0 & 0 & 0 & 2.9 & 0 \\ 0 & 0 & 0 & 3.5 & 0 & 0 & 0 & 3.2 \\ 2.5 & 0 & 0 & 0 & 6.5 & 0 & 0 & 0 \\ 0 & 2.7 & 0 & 0 & 0 & 7.6 & 0 & 0 \\ 0 & 0 & 2.9 & 0 & 0 & 0 & 8.8 & 0 \\ 0 & 0 & 0 & 3.2 & 0 & 0 & 0 & 10.7 \end{bmatrix}. \quad (74)$$

4.2.1 | Outer-loop control

For an outer-loop control, the NDI based SMC law is chosen as

$$u_s(t) = g_s^{-1}(x_r)\left(\nu_s(t) - f_s(x_r) + \nu_{s_n}(t)\right) \quad (75)$$

where $g_s^{-1}(x_r)$ exists except $\phi, \theta = \pm\pi/2$, therefore, the range of ϕ and θ are restricted to $-\pi/2 < \phi, \theta < \pi/2$. In fact from practical perspective this is acceptable assumption as octorotor is restricted for having 90° roll and pitch maneuvering. This assumption is also made in Reference 52. In (75), $\nu_{s_n}(t)$ is the SMC law defined as

$$\nu_{s_n}(t) = -\Gamma_s \frac{S_s(t)}{S_s(t)}, \quad \text{for all } S_s(t) \neq 0 \quad (76)$$

where Γ_s is the modulation gain selected as $\Gamma_s \geq \|D_s\Phi_s(x_s, t)\|$ and $S_s(t)$ is the switching surface defined as

$$S_s(t) = x_{s_d}(t) - x_s(t) \quad (77)$$

where $x_{s_d}(t)$ denotes the desired state vector and is defined as $x_{s_d}(t) = col(x_{ed}, y_{ed})$ and $\nu_s(t)$ is the virtual outer-loop control law that determines the desired dynamics and is defined as

$$\nu_s(t) = \begin{cases} \ddot{x}_{ed} + K_{x_1}(\dot{x}_{ed} - \dot{x}_e) + K_{x_2}(x_{ed} - x_e) \\ \ddot{y}_{ed} + K_{y_1}(\dot{y}_{ed} - \dot{y}_e) + K_{y_2}(y_{ed} - y_e) \end{cases} \quad (78)$$

where x_{ed} and y_{ed} are the desired reference signals. In (78), the gains are chosen as $K_{x_1}, K_{y_1} = 0.5$ and $K_{x_2}, K_{y_2} = 5$. Note that the outer-loop bandwidth is chosen smaller than the bandwidth of actuator and inner-loop system bandwidth.

4.3 | Simulation results

In this section, a detailed simulation is carried out on the nonlinear coaxial octorotor UAV system and comparison is performed with scheme given in Reference 59. The existing method[59] requires no-fault information to reconfigure the nominal control law and a fixed sliding gain is chosen throughout the system response. In the nonlinear simulations, several real-time effects are included to check the suitability of the actuator FTC scheme in real-time flight conditions.

4.3.1 | Fault free condition

In this subsection, the simulations are performed in the fault-free condition. The performance is analyzed by applying a triangular reference altitude command of 6 m amplitude and the yaw angle is set to 0°. Two multi-steps input signals are applied as $x-y$ reference input to the outer-loop subsystem which in return generates the desired roll and pitch setting to

10991239, 2021, 6, Downloaded from https://onlinelibrary.wiley.com/doi/10.1002/rnc.5394 by University Of Maryland, Wiley Online Library on [05/03/2024]. See the Terms and Conditions (https://onlinelibrary.wiley.com/terms-and-conditions) on Wiley Online Library for rules of use; OA articles are governed by the applicable Creative Commons License

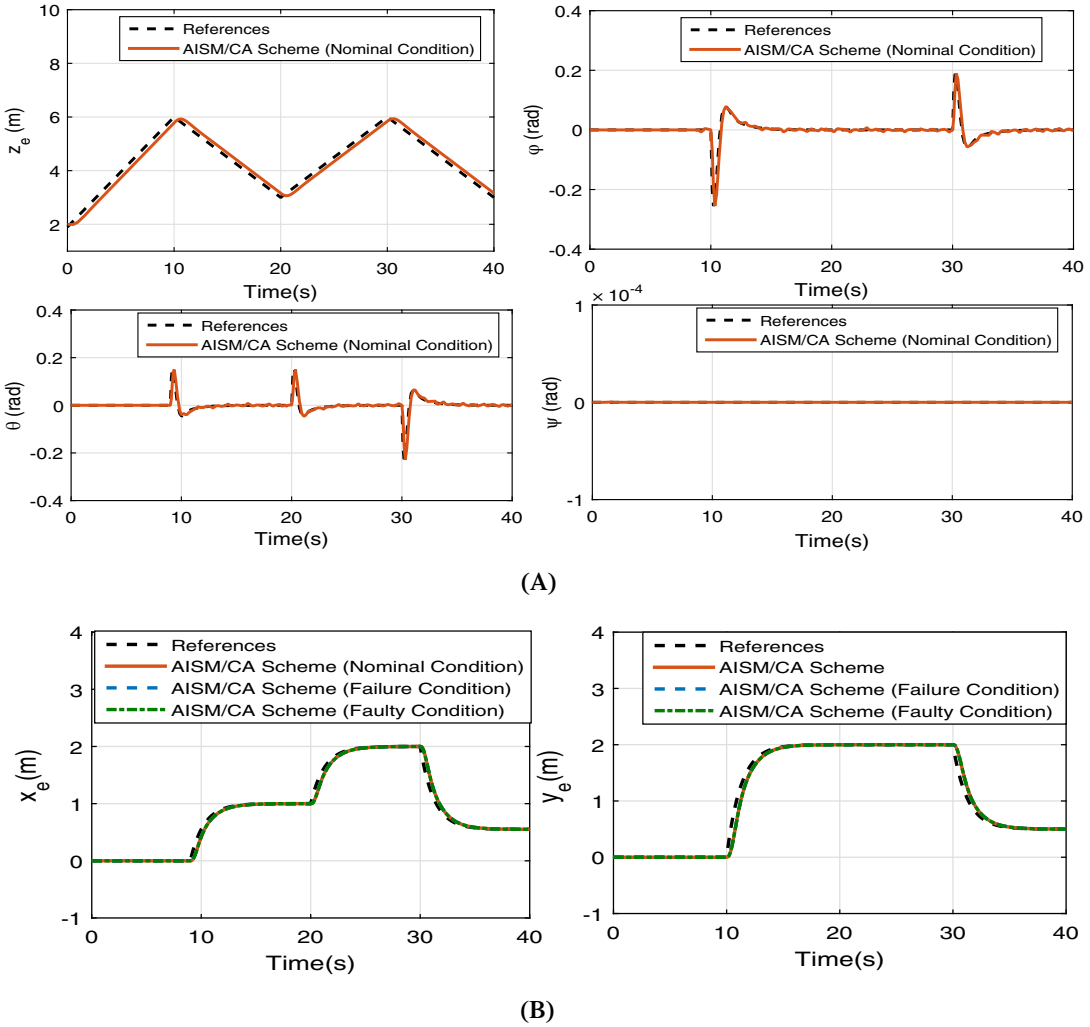

FIGURE 4 Performance analysis in fault free condition. (A) Altitude and attitude maneuvering. (B) $x-y$ tracking [Colour figure can be viewed at wileyonlinelibrary.com]

FIGURE 5 Adaptive control law and switching function in fault free condition [Colour figure can be viewed at wileyonlinelibrary.com]

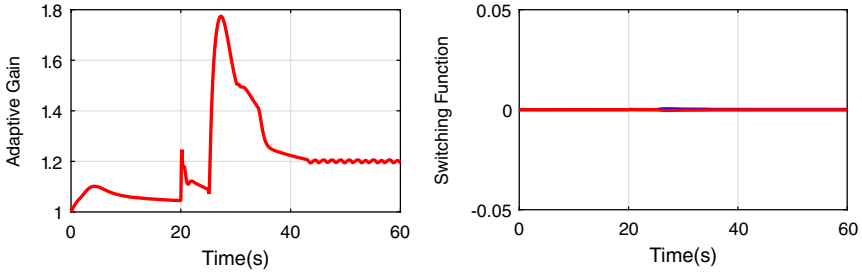

inner-loop subsystem $x_r(t)$. The desired forces/torque, as demanded by the controller, is applied to actuator dynamics. The actual force/torque and consequently the speed is provided by the actuator dynamics which is then applied to the octorotor input. It can be seen from Figure 4(A) that the proposed actuator FTC scheme provides accurate command tracking in fault-free condition. The outer-loop tracking response in Figure 4(B) shows the reference maneuvering is accomplished by using the NDI based SMC strategy. It follows from Figure 7(A,B) that all the actuators are equally contributing towards desired flight path. The plots of the switching function and adaptive gain are shown in Figure 5. The increasing gain counters the disturbance and the uncertainty effect. However, when the sliding motion reaches below the threshold value ϵ, the gain returns to the initial value and rises again when the sliding motion slides away from the prescribed threshold point ϵ.

10991239, 2021, 6, Downloaded from https://onlinelibrary.wiley.com/doi/10.1002/rnc.5394 by University Of Maryland, Wiley Online Library on [05/03/2024]. See the Terms and Conditions (https://onlinelibrary.wiley.com/terms-and-conditions) on Wiley Online Library for rules of use; OA articles are governed by the applicable Creative Commons License

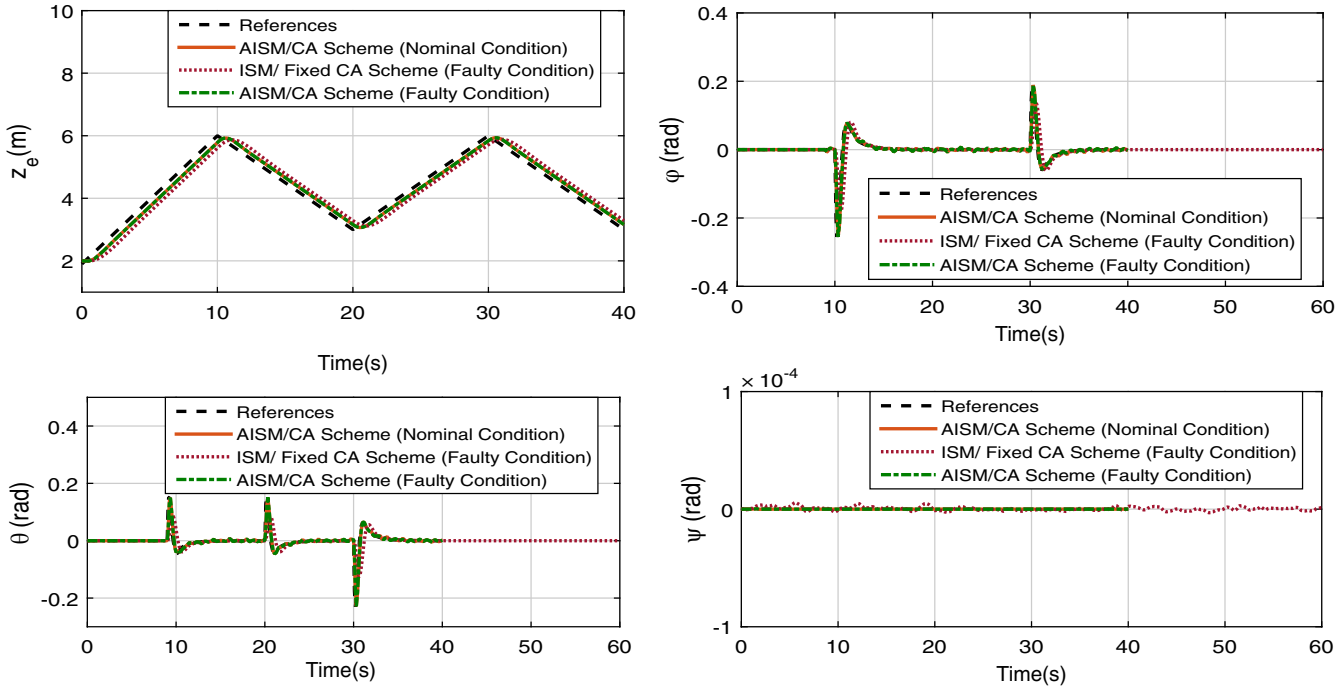

FIGURE 6 Performance analysis in faulty condition. Altitude and attitude maneuvering tracking [Colour figure can be viewed at wileyonlinelibrary.com]

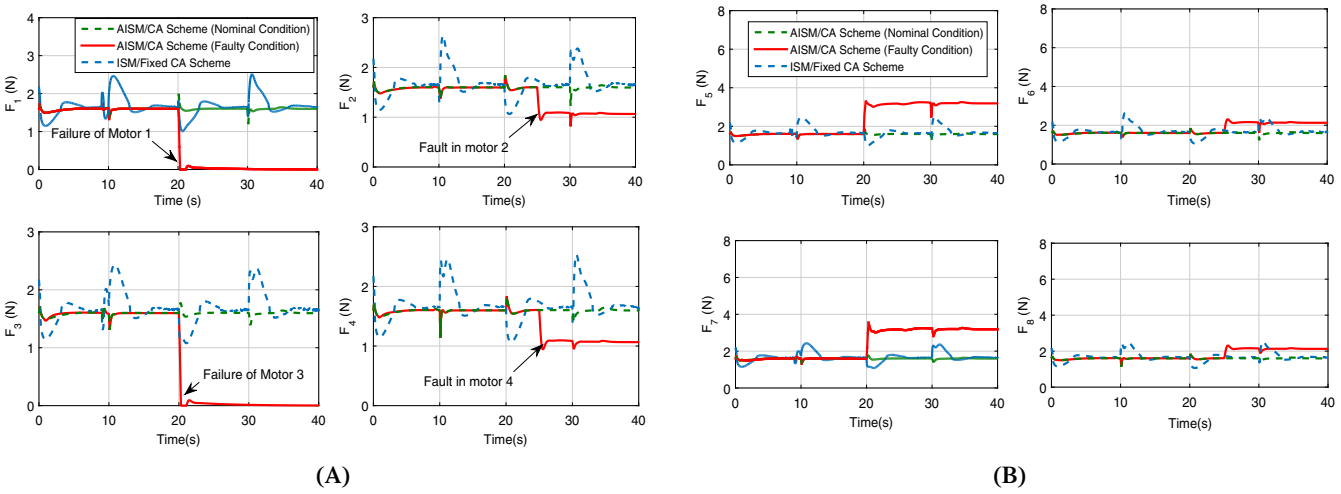

FIGURE 7 Performance analysis in faulty condition. (A) Thrust generated by the motor 1 – 4. (B) Thrust generated by motor 5 – 8. [Colour figure can be viewed at wileyonlinelibrary.com]

4.3.2 | Tracking performance analysis in fault-failure combination

In this scenario, the rotors 1 and 3 are subjected to the complete failure after 20 seconds, and the rotors 2 and 4 are subject to 50% loss-in-effectiveness. The estimate of the effectiveness level of rotors is provided by fault estimation unit. The tracking plots are given in Figure 6 which show no visible difference in performance of the proposed strategy from the nominal condition and fixed CA scheme. The allocation of control input to each rotor is given in Figure 7(A). It is clear that in the case of the proposed strategy, the failed actuators are not contributing to flight operation after 20 seconds, whereas the faulty actuators provide less control effort to the system. To maintain the flight path, the online CA scheme distributes more control signals to the associated healthy pairs as shown in Figure 7(B). The adaptive sliding gain and

10991239, 2021, 6, Downloaded from https://onlinelibrary.wiley.com/doi/10.1002/rnc.5394 by University Of Maryland, Wiley Online Library on [05/03/2024]. See the Terms and Conditions (https://onlinelibrary.wiley.com/terms-and-conditions) on Wiley Online Library for rules of use; OA articles are governed by the applicable Creative Commons License

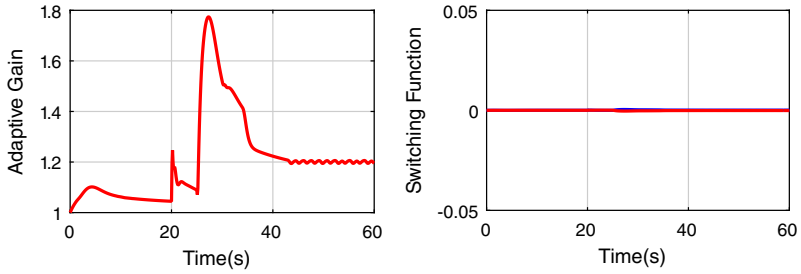

FIGURE 8 Adaptive control law and switching function in faulty condition [Colour figure can be viewed at wileyonlinelibrary.com]

switching function in Figure 8, shows the adaptive modulation gain increases to mitigate external disturbance and uncertainty.

4.3.3 | Tracking performance analysis in rotors failure condition

In this simulation, the rotors 1 and 2 are exposed to the failure after 15 seconds, whereas the rotors 3 and 4 failure occurred after 30 seconds. The failure information is shown in Figure 9(B). The CA scheme responded immediately to the failure and redistributes the control input signals to the available healthy pairs. The tracking performance of the proposed strategy is also comparable with that of the nominal condition as shown in Figure 9(A). However, the performance deviates a little from the nominal set-point in existing FTC strategy. This is because that the fixed CA scheme has no information of failed rotors. However, due to the sufficient redundancy available in the system, the tracking path, although not very perfect but still achievable. The control effort provided by each rotor is given in Figure 10(A,B). Notable that in case of the proposed strategy, the failed rotors (1 and 2) are not contributing and their effectiveness level is reduced to zero after 15 and 30 seconds. However, the control efforts of the failed rotor are provided by the associated rotor pairs as shown in Figure 10(B). However, the existing controller has no information about the rotor failure. Therefore, the controller is still providing the desired control effort to the system. The plots of adaptive gain is provided in Figure 11which shows that increasing trend in the modulation gain after 15 and 30 seconds. This is because the failed actuator causes the transient in the state trajectories. To cope with such transient effect, the adaptive gain rises to keep the state trajectories back to the sliding manifold.

4.3.4 | Tracking performance in the presence of wind -gust

In this subsection, a practical case is considered by adding the wind-gust condition (Section 3.2) in the nonlinear simulations. The performance of the proposed scheme is tested in worst-case scenario, that is, failure of rotors 1 and 3 at 15 seconds and rotors 2 and 4 failure after 25 seconds. From the reference tracking results shown in Figure 12(A,B), it can be visualized that despite a little deviation from the reference input due to the effect of wind, the position tracking is still attained. The effect of wind on the motor dynamics can be evident from plots of thrust generated by the motors provided in Figure 13(A,B). It can also be analyzed that the control efforts of failed rotors $(1-4)$ are distributed among the healthy redundant rotors $(5-8)$. The plots of adaptive gain and switching function are given in Figure 14 that clearly shows that adaptive gain rises to cater to the uncertainty and wind-gust effects. Consequently, the sliding motion is maintained into the sliding surface.

4.3.5 | Tracking performance analysis subject to sensor noise and model uncertainty

In this subsection, the robustness of the actuator FTC scheme is tested by including the sensor noise and model parameters uncertainty as provided in Table 1. The tracking performance comparison subject to the three different parameter varying conditions is provided in Figure 15(A,B). It can be visualized in Figure 16 that the controller attempts to keep the octorotor following the desired flight path even with the variation of system parameters. However, a minor deterioration in the performance can be seen in the case of a 15% variation in system parameters. The plots of adaptive gain and switching

10991239, 2021, 6, Downloaded from https://onlinelibrary.wiley.com/doi/10.1002/rnc.5394 by University Of Maryland, Wiley Online Library on [05/03/2024]. See the Terms and Conditions (https://onlinelibrary.wiley.com/terms-and-conditions) on Wiley Online Library for rules of use; OA articles are governed by the applicable Creative Commons License

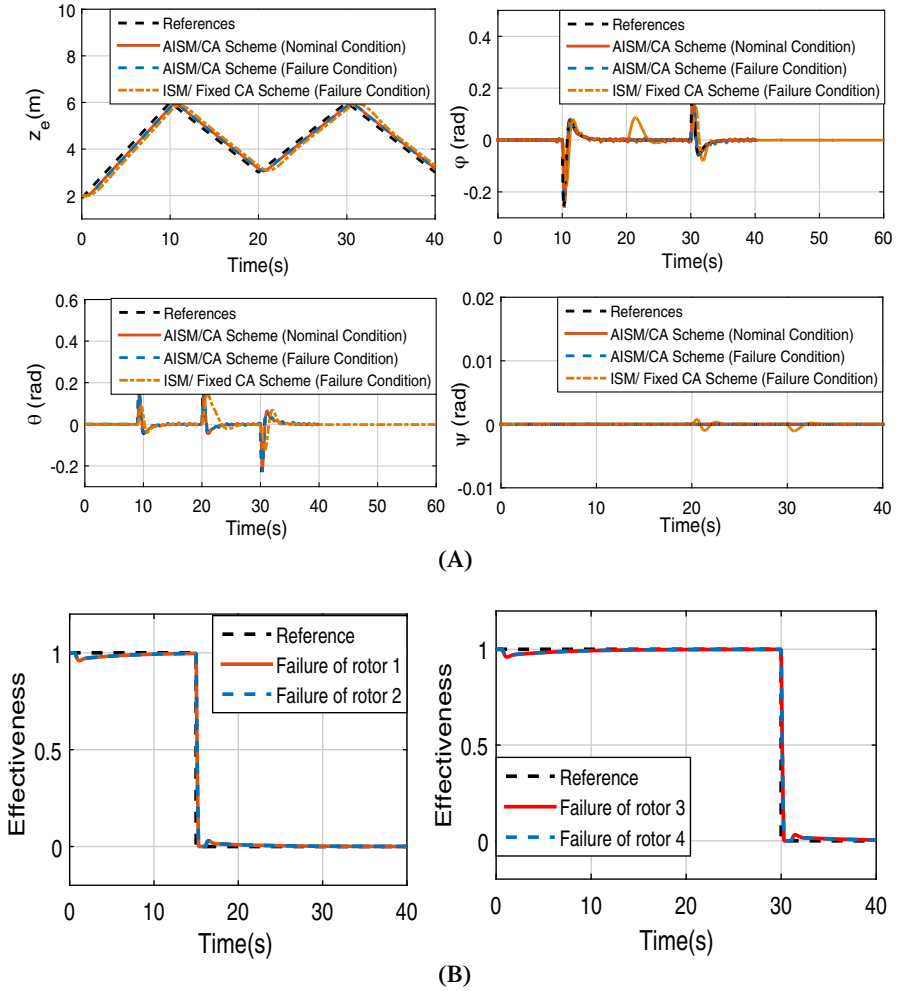

FIGURE 9 Performance analysis in failure condition. (A) Altitude and attitude maneuvering. (B) Estimate of actuator effectiveness [Colour figure can be viewed at wileyonlinelibrary.com]

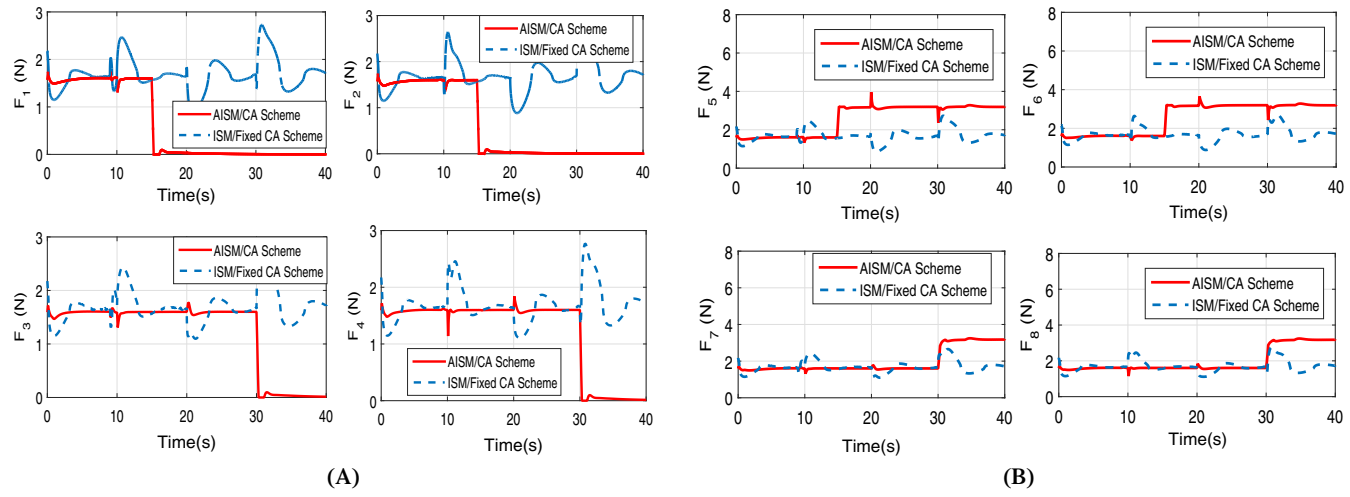

FIGURE 10 Performance analysis in total failure condition. (A) Thrust generated by the motor 1 – 4. (B) Thrust generated by motor 5 – 8 [Colour figure can be viewed at wileyonlinelibrary.com]

10991239, 2021, 6, Downloaded from https://onlinelibrary.wiley.com/doi/10.1002/rnc.5394 by University Of Maryland, Wiley Online Library on [05/03/2024]. See the Terms and Conditions (https://onlinelibrary.wiley.com/terms-and-conditions) on Wiley Online Library for rules of use; OA articles are governed by the applicable Creative Commons License

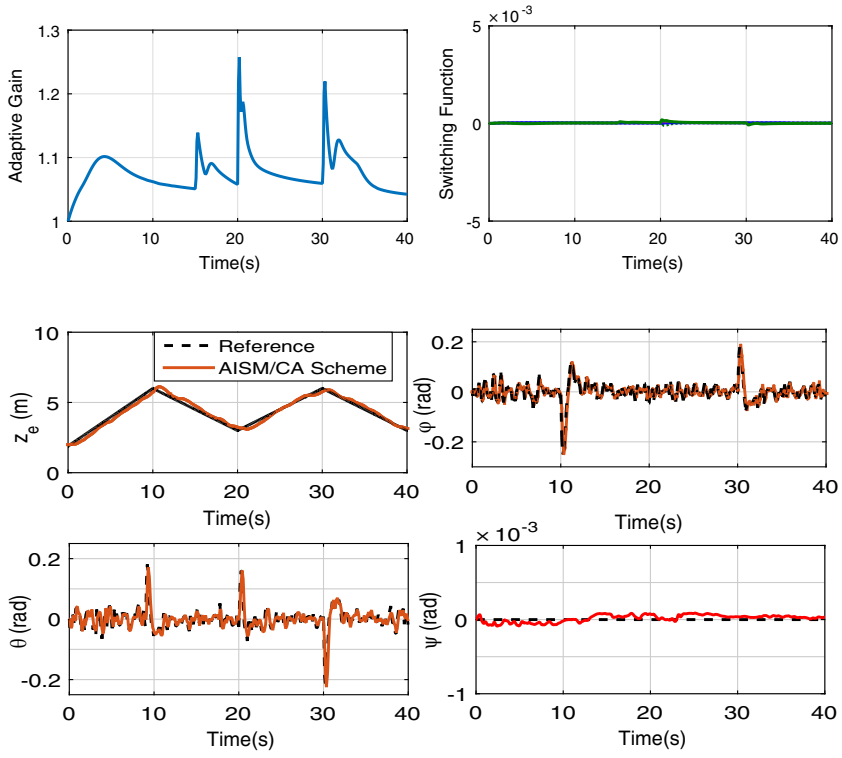

FIGURE 11 Adaptive control law and switching function in total failure condition [Colour figure can be viewed at wileyonlinelibrary.com]

FIGURE 12 Performance analysis in wind-gust condition. (A) Altitude and attitude maneuvering. (B) $x-y$ positioning [Colour figure can be viewed at wileyonlinelibrary.com]

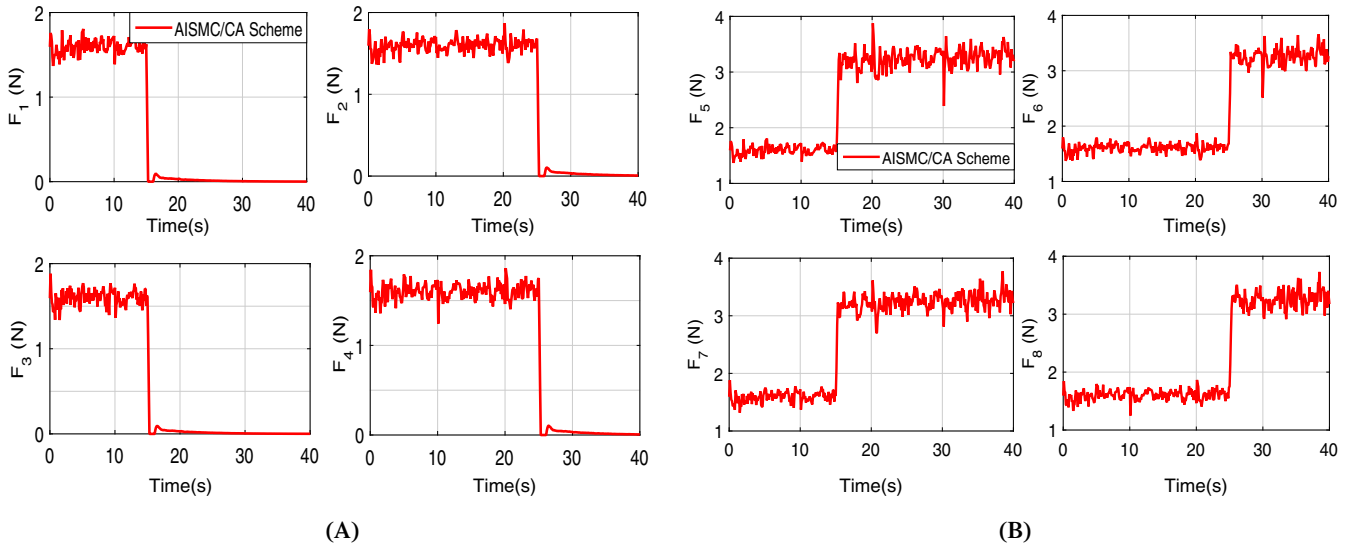

FIGURE 13 Performance analysis in wind-gust condition. (A) Thrust generated by the motor 1 – 4. (B) Thrust generated by motor 5 – 8 [Colour figure can be viewed at wileyonlinelibrary.com]

10991239, 2021, 6, Downloaded from https://onlinelibrary.wiley.com/doi/10.1002/rnc.5394 by University Of Maryland, Wiley Online Library on [05/03/2024]. See the Terms and Conditions (https://onlinelibrary.wiley.com/terms-and-conditions) on Wiley Online Library for rules of use; OA articles are governed by the applicable Creative Commons License

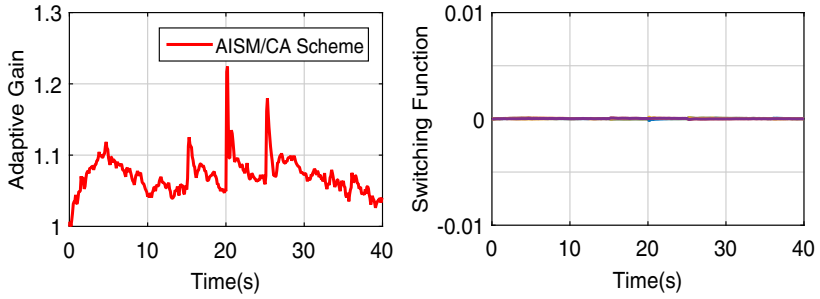

FIGURE 14 Adaptive control law and switching function in wind-gust condition [Colour figure can be viewed at wileyonlinelibrary.com]

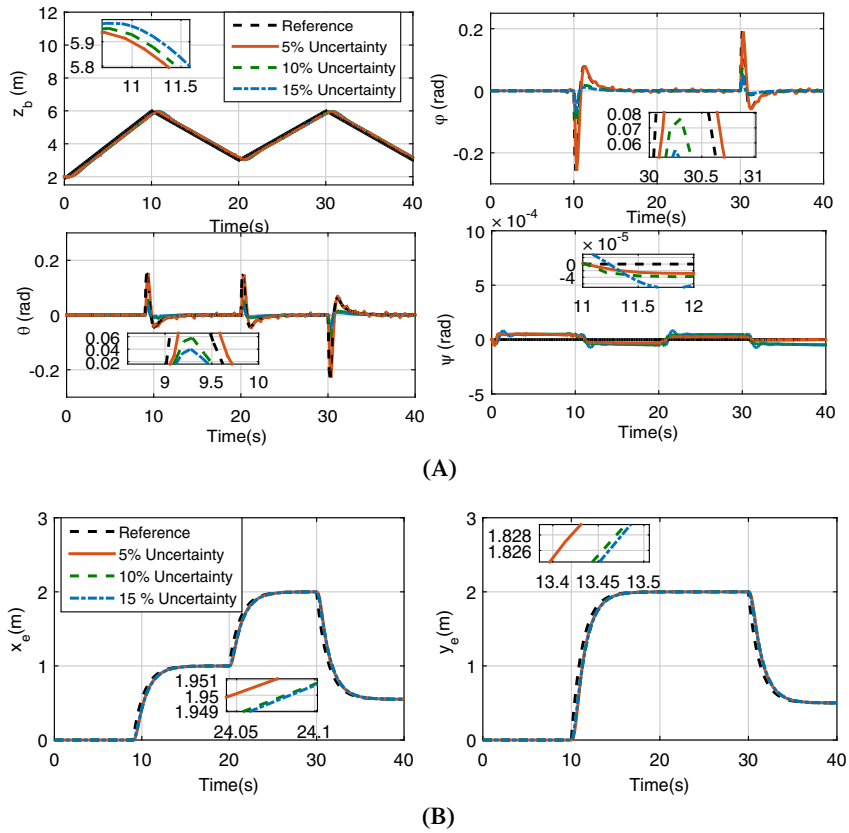

FIGURE 15 Performance analysis in the presence of sensor noise and parameter variation. (A) Altitude and attitude maneuvering. (B) $x-y$ position control [Colour figure can be viewed at wileyonlinelibrary.com]

function in Figure 17 show that with an increase in the percentage of parameter uncertainty, the adaptive gain rises to maintain the sliding motion.

4.3.6 | Tracking performance analysis in output feedback frame

In this analysis, the estimated states $\hat{x}_r(t)$ information from the observer (70) is applied to the final control law (59), and tracking performance is analyzed both in nominal and failure conditions. The altitude and attitude maneuvering results are provided in Figure 18(A,B). It can be evident that set-point tracking is attained both in nominal and failure conditions despite the estimated states are fed to the final control law. The distribution of control input signals both in nominal and actuators failure conditions are given in Figure 19(A,B) which clearly shows that control signals are redistributed by CA scheme when the failure of rotors 1-4 occurred after 15 and 30 seconds. The plots of adaptive gain and switching function are given in Figure 20. It can be seen that the sliding motion is maintained both in nominal and failure conditions.

10991239, 2021, 6, Downloaded from https://onlinelibrary.wiley.com/doi/10.1002/rnc.5394 by University Of Maryland, Wiley Online Library on [05/03/2024]. See the Terms and Conditions (https://onlinelibrary.wiley.com/terms-and-conditions) on Wiley Online Library for rules of use; OA articles are governed by the applicable Creative Commons License

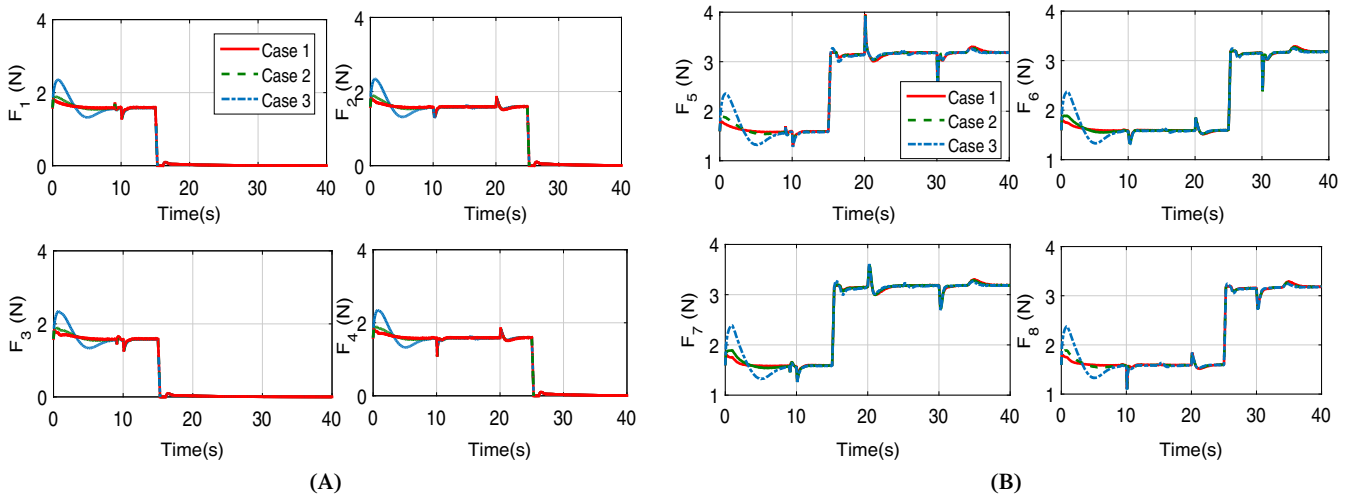

FIGURE 16 Performance analysis in the presence of sensor noise and parameter variation. (A) Thrust generated by the motor 1 – 4. (B) Thrust generated by motor 5 – 8 [Colour figure can be viewed at wileyonlinelibrary.com]

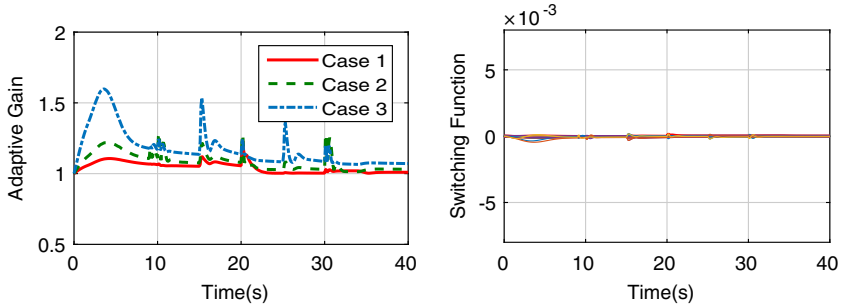

FIGURE 17 Adaptive control law and switching function in parameter uncertainty condition and sensor noise [Colour figure can be viewed at wileyonlinelibrary.com]

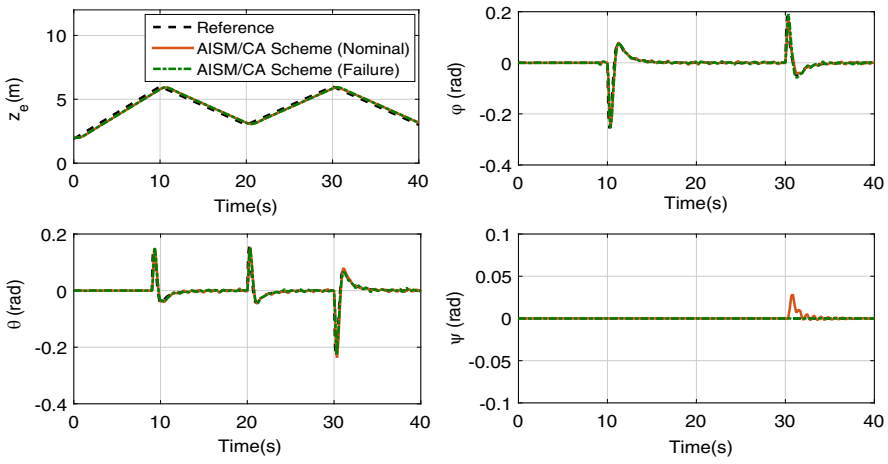

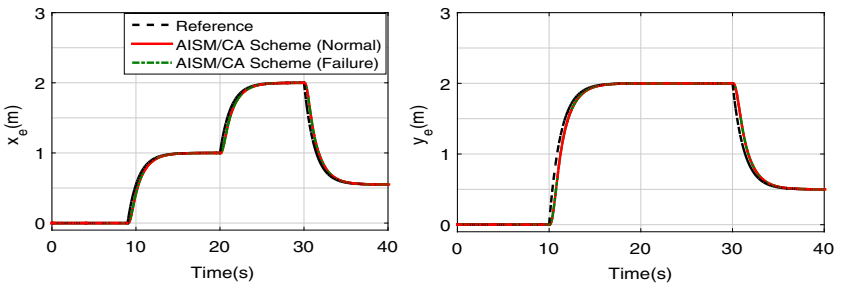

FIGURE 18 Performance analysis in nominal and failure conditions with estimated states. (A) Altitude and attitude maneuvering. (B) $x - y$ position control [Colour figure can be viewed at wileyonlinelibrary.com]

10991239, 2021, 6, Downloaded from https://onlinelibrary.wiley.com/doi/10.1002/rnc.5394 by University Of Maryland, Wiley Online Library on [05/03/2024]. See the Terms and Conditions (https://onlinelibrary.wiley.com/terms-and-conditions) on Wiley Online Library for rules of use; OA articles are governed by the applicable Creative Commons License

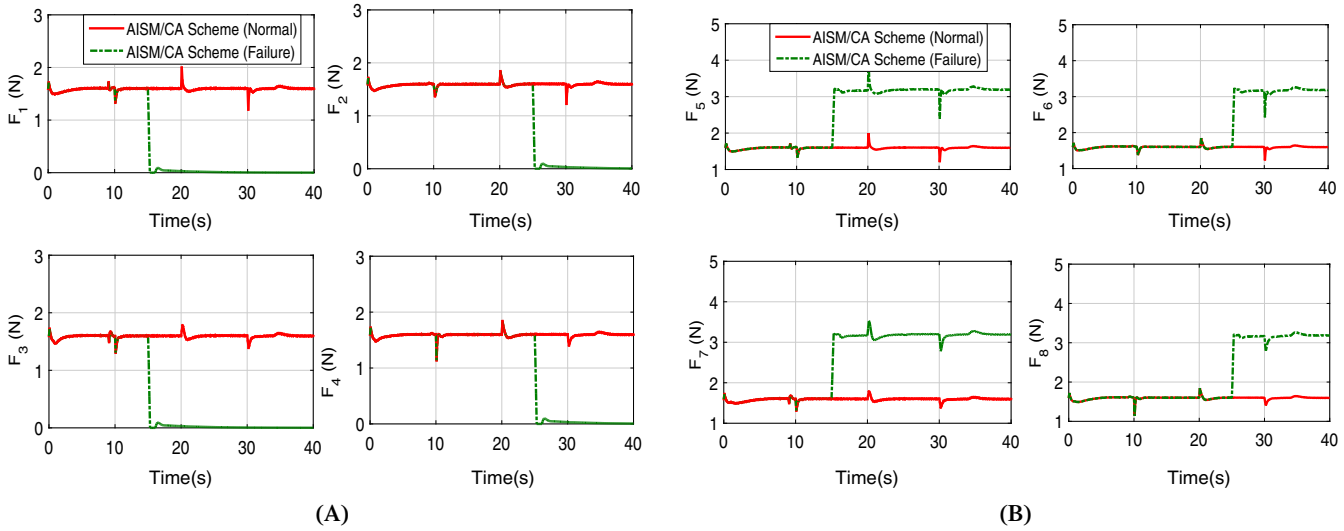

FIGURE 19 Performance analysis in nominal and failure conditions with estimated states. (A) Thrust generated by the motor 1 – 4. (B) Thrust generated by motor 5 – 8 [Colour figure can be viewed at wileyonlinelibrary.com]

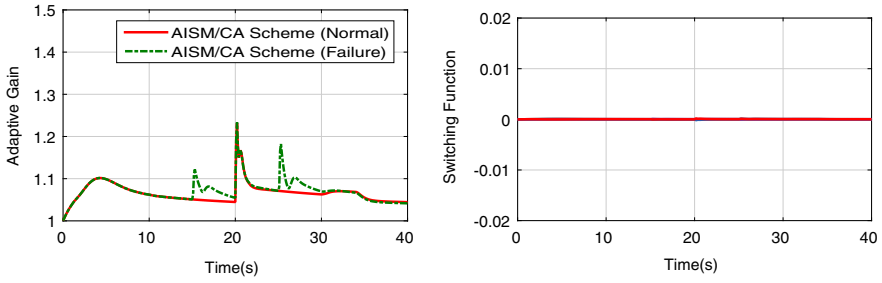

FIGURE 20 Adaptive control law and switching function in nominal and failure conditions with estimated states [Colour figure can be viewed at wileyonlinelibrary.com]

5 | CONCLUSION

This article proposes a new adaptive ISM FTC scheme for over-actuated Lipschitz nonlinear systems. The designed method combines the robustness property of ISMC law with CA scheme and adaptive strategy to effectively manage the actuator redundancy subject to the presence of unknown disturbance, uncertainty arises in the system due to faults and failures, input matrix approximation error, and fault estimation error. A closed-loop stability analysis is performed to ensure the convergence of state trajectories to the sliding manifold and stability conditions are derived using LMI technique. The performance of the proposed scheme is validated on the octorotor UAV system and results are compared with the fixed ISMC based CA method in the literature. The stability of internal dynamics (outer-loop) is ensured using NDI based SMC strategy. Simulations on nonlinear system validated the performance of proposed FTC scheme closer to nominal system. In the future work, the problem of output feedback stabilization will be considered in which the estimated states from the observer is used in the controller design part and closed-loop stability analysis is performed subject to actuator faults and failure.

ORCID

Salman Ijaz https://orcid.org/0000-0003-1483-4754
Fuyang Chen https://orcid.org/0000-0003-2650-420X

REFERENCES

1. Montes de Oca S, Tornil-Sin S, Puig V, Theilliol D. Fault-tolerant control design using the linear parameter varying approach. *Int J Robust Nonlinear Control*. 2014;24:1969-1988.
2. Abdolah S, Zahra K. Robust fault-tolerant controller design for aerodynamic load simulator. *Aerosp Sci Technol*. 2018;78(1):332-341.
3. Nasiri A, Nguang SK, Swain A, Almakhles D. Passive actuator fault tolerant control for a class of MIMO nonlinear systems with uncertainties. *Int J Control*. 2019;2(3):693-704.

10991239, 2021, 6, Downloaded from https://onlinelibrary.wiley.com/doi/10.1002/rnc.5394 by University Of Maryland, Wiley Online Library on [05/03/2024]. See the Terms and Conditions (https://onlinelibrary.wiley.com/terms-and-conditions) on Wiley Online Library for rules of use; OA articles are governed by the applicable Creative Commons License

4. Li Y, Yang G. Robust fuzzy adaptive fault-tolerant control for a class of nonlinear systems with mismatched uncertainties and actuator faults. *Nonlinear Dyn*. 2015;81:395-409.
5. Mammadov H, Hajiyev C. Reconfigurable fault tolerant flight control for UAV with pseudo-inverse technique. *IFAC-Papers OnLine*. 2018;51(30):83-88.
6. Yan L, Yang GH, Li XJ. Fault-tolerant control for uncertain linear systems via adaptive and LMI approaches. *Int J Syst Sci*. 2017;48(2):347-356.
7. Lee TH, Lim CP, Nahavandi S, Roberts RG. Observer-based $\mathcal{H}_\infty$ fault-tolerant control for linear systems with sensor and actuator faults. *IEEE Syst J*. 2018;13(2):1981-1990.
8. Wang J, Wang S, Wang X, Shi C, Tomovic MM. Active fault tolerant control for vertical tail damaged aircraft with dissimilar redundant actuation system. *Chin J Aeronaut*. 2016;29(5):1313-1325.
9. Rabaoui B, Hamdi H, Benhadj NB, Rodrigues M. A reconfigurable PID fault tolerant tracking controller design for LPV systems. *ISA Trans*. 2020;98:173-185.
10. Rodrigues M, Hamdi H, Braiek NB, Theilliol D. Observer-based fault tolerant control design for a class of LPV descriptor systems. *J Frankl Inst*. 2014;351(6):3104-3125.
11. Rotondo A, Ponsart JC, Theilliol D, Nejjari F, Puig V. Fault tolerant control of unstable LPV systems subject to actuator saturation using virtual actuators. *IFAC-PapersOnLine*. 2015;48(21):18-23.
12. Shi F, Patton RJ. Fault estimation and active fault tolerant control for linear parameter varying descriptor systems. *Int J Robust Nonlinear Control*. 2015;25:689-706.
13. Durham WC. Constrained control allocation. *J Guid Control Dyn*. 1993;16(4):717-725.
14. Zhang YM, Suresh VS, Jiang B, Theilliol D. Reconfigurable control allocation against aircraft control effector failures. Paper presented at: Proceedings of the 2007 IEEE International Conference on Control Applications. Singapore: IEEE; 2007:1197-1202.
15. Zhang YM, Rabbath CA, Su CY. Reconfigurable control allocation applied to an aircraft benchmark model. Paper presented at: Proceedings of the 2008 American Control Conference, Seattle, WA; 2008:1052-1057.
16. Alwi H, Edwards C. Fault tolerant control using sliding modes with on-line control allocation. *Automatica*. 2008;44(7):1859-1866.
17. Alwi H, Edward C. Fault detection and fault-tolerant control of a civil aircraft using a sliding-mode-based scheme. *IEEE Trans Control Syst Technol*. 2008;16(3):499-510.
18. Hamayun MT, Edwards C, Alwi H. *Fault Tolerant Control Schemes Using Integral Sliding Modes*. Cham, Switzerland: Springer; 2016.
19. Argha A, Su SW, Celler BG. Control allocation-based fault tolerant control. *Automatica*. 2019;103:408-417.
20. Utkin V, Poznyak A, Orlov YV, Polyakov A. *Road Map for Sliding Mode Control Design*. Springer Briefs in Mathematics. 1st ed. New York, NY: Springer; 2020.
21. Argha A, Su SW, Zheng WX, Celler BG. Sliding-mode fault-tolerant control using the control allocation scheme. *Int J Robust Nonlinear Control*. 2019;29:6256-6273.
22. Lejun C, Christopher E, Halim A, Masayuki S. Flight evaluation of a sliding mode online control allocation scheme for fault tolerant control. *Automatica*. 2020;114:108829.
23. Argha A, Su SW, Celler BG. Static output feedback fault tolerant control using control allocation scheme. *Int J Robust Nonlinear Control*. 2019;29:98-116.
24. Alwi H, Edwards C. Sliding mode fault-tolerant control of an octorotor using linear parameter varying-based schemes. *IET Control Theory Appl*. 2015;9(4):618-636.
25. Ijaz I, Yan L, Humayun MT, Cun S. Active fault tolerant control scheme for aircraft with dissimilar redundant actuation system subject to hydraulic failure. *J Frankl Inst*. 2019;356(3):1302-1332.
26. Hamayun MT, Ijaz S, Bajodah AH. Output integral sliding mode fault tolerant control scheme for LPV plants by incorporating control allocation. *IET Control Theory Appl*. 2017;11(12):1959-1967.
27. Huang Y, Kuo T, Chang T. Adaptive sliding-mode control for nonlinear systems with uncertain parameters. *IEEE Trans Syst Man Cybern Part B (Cybern)*. 2008;38(2):534-539.
28. Utkin VI, Poznyak AS. *Adaptive sliding mode control*. In: Bandyopadhyay B, Janardhanan S, Spurgeon S, eds. *Advances in Sliding Mode Control*. Lecture Notes in Control and Information Sciences. Berlin/Heidelberg, Germany: Springer; 2013.
29. Wang B, Zhang Y. Anadaptive fault-tolerant sliding mode control allocation scheme for multirotor helicopter subject to simultaneous actuator faults. *IEEE Trans Ind Electron*. 2018;65(5):4227-4236.
30. Rajamani R. Observers for Lipschitz nonlinear systems. *IEEE Trans Autom Control*. 1998;43(3):397-401.
31. Pertew AM, Marquez HJ, Zhao QH. ∞ observer design for Lipschitz nonlinear systems. *IEEE Trans Autom Control*. 2006;51(7):1211-1216.
32. Yadegar M, Afshar A, Davoodi M. Observer-based tracking controller design for a class of Lipschitz nonlinear systems. *J Vib Control*. 2018;24(11):12-19.
33. Zhang W, Su H, Zhu F, Ghassan MA. Unknown input observer design for one-sided Lipschitz nonlinear systems. *Nonlinear Dyn*. 2015;79:1469-1479.
34. Mohsen E. Observer-based controller for Lipschitz nonlinear systems. *Int J Syst Sci*. 2017;48(16):3411-3418.
35. Carlos ES, Robust H. ∞ filtering for a class of discrete-time Lipschitz nonlinear system. *Automatica*. 2019;103:69-80.
36. Khosrowjerdi MJ. Mixed H2/H∞ approach to fault-tolerant controller design for Lipschitz non-linear systems. *IET Control Theory Appl*. 2011;5(2):299-307.
37. Khosrowjerdi MJ, Barzegary S. Fault tolerant control using virtual actuator for continuous-time Lipschitz nonlinear systems. *Int J Robust Nonlinear Control*. 2014;24(16):2597-2607.

10991239, 2021, 6, Downloaded from https://onlinelibrary.wiley.com/doi/10.1002/rnc.5394 by University Of Maryland, Wiley Online Library on [05/03/2024]. See the Terms and Conditions (https://onlinelibrary.wiley.com/terms-and-conditions) on Wiley Online Library for rules of use; OA articles are governed by the applicable Creative Commons License

38. Azmi H, Khosrowjerdi MJ. Robust adaptive fault tolerant control for a class of Lipschitz nonlinear systems with actuator failure and disturbances. *Proc Inst Mech Eng Part I J Syst Control Eng*. 2016;230(1):13-22.
39. Rastegari A, Arefi MM, Asemani MH. Robust H∞ sliding mode observer-based fault-tolerant control for one-sided Lipschitz nonlinear systems. *Asian J Control*. 2019;21:114-129.
40. Hmidi R, Brahim AB, Hmida FB, Sellami A. Robust fault tolerant control design for nonlinear systems not satisfying matching and minimum phase conditions. *Int J Control Autom Syst*. 2020;18:2206-2219.
41. Ijaz S, Chen F, Hamayun MT, Yan L, Shi C. An adaptive integral sliding mode FTC scheme for dissimilar redundant actuation system of civil aircraft. *Int J Syst Sci*. 2019;50(14):2687-2702.
42. Ijaz S, Yan L, Humayun MT, Baig WM, Chi S. Adaptive LPV integral sliding mode FTC scheme for dissimilar redundant actuation system for civil aircraft. *IEEE Access*. 2018;6:65960-65973.
43. Khalil HK. *Nonlinear Systems*. Upper Saddle River, NJ: Prentice Hall; 1992.
44. Golub GH, Loan VCF. *Matrix Computations*. Baltimore, MD: Johns Hopkins University Press; 2012.
45. Pagilla PR, Zhu Y. Controller and observer design for Lipschitz nonlinear systems. Paper presented at: Proceedings of the American Control Conference; vol. 3, 2004:2379-2384; Boston, MA.
46. Castanos F, Fridman L. Analysis and design of integral sliding manifolds for systems with unmatched perturbations. *IEEE Trans Autom Control*. 2006;51(5):853-858.
47. Stephen B, Laurent EG, Eric F, Venkataramanan B. *Linear Matrix Inequalities in System and Control Theory*. Philadelphia, PA: SIAM Studies in Applied Mathematics; 2002.
48. Lee H, Utkin VI. Chattering suppression methods in sliding mode control systems. *Annu Rev Control*. 2007;31:179-188.
49. Hao W, Xian B. Nonlinear adaptive fault-tolerant control for a quadrotor UAV based on immersion and invariance methodology. *Nonlinear Dyn*. 2017;90:2813-2826.
50. Liu H, Derawi D, Kim J, Yisheng Z. Robust optimal attitude control of hexarotor robotic vehicles. *Nonlinear Dyn*. 2013;74:1155-1168.
51. Adir VG, Stoica AM. Integral LQR control of a star-shaped octorotor. *INCAS Bull*. 2012;4(2):3-18.
52. Alwi H, Edwards C. Fault tolerant control of an octorotor using LPV based sliding mode control allocation. Paper presented at: Proceedings of the American Control Conference; 2013:6505-6510; Washington, DC.
53. Wang B, Zhang Y. An adaptive fault-tolerant sliding mode control allocation scheme for multirotor helicopter subject to simultaneous actuator Fdults. *IEEE Trans Ind Electron*. 2018;65(5):4227-4236.
54. Zeghlache S, Mekki H, Bouguerra A, Djerioui A. Actuator fault tolerant control using adaptive RBFNN fuzzy sliding mode controller for coaxial octorotor UAV. *ISA Trans*. 2018;80:267-278.
55. Hoblit F. Gust Loads on Aircraft: Concepts and Applications, AIAA Education Series; 1988.
56. Department of Defense Handbook, MIL-HDBK-1797B, Washington, DC: U.S. Department of Defense, Flying Qualities of Piloted Aircraft; 2012
57. Ansari U, Bajodah AH, Hamayun MT. Quadrotor control via robust generalized dynamic inversion and adaptive non-singular terminal sliding mode. *Asian J Control*. 2019;21:1237-1249.
58. Chen F, Jiang R, Zhang K, Jiang B, Tao G. Robust backstepping sliding-mode control and observer-based fault estimation for a quadrotor UAV. *IEEE Trans Ind Electron*. 2016;63(8):5044-5056.
59. Hamayun MT, Edwards C, Alwi H, Bajodah ARA. fault tolerant direct control allocation scheme with integral sliding modes. *Int J Appl Math Comput Sci*. 2015;25(1):93-102.
60. Utkin VI, Poznyak AS. Adaptive sliding mode control with application to super-twist algorithm: equivalent control method. *Automatica*. 2013;49(1):39-47.

How to cite this article: Ijaz S, Chen F, Tariq Hamayun M. A new actuator fault-tolerant control for Lipschitz nonlinear system using adaptive sliding mode control strategy. *Int J Robust Nonlinear Control*. 2021;31:2305–2333. https://doi.org/10.1002/rnc.5394

APPENDIX

Consider a Lyapunov function

$$V_r(t) = \frac{1}{2} S_r^T(t) S_r(t) \tag{A1}$$

and the time derivative after substituting (31), (35) and (18) is written as

$$\dot{V}_r(t) = S_r^T(t)(B_{l_2}(1 - \Delta(t))B_{l_2}^+(t)(\nu_{fl}(t) + \nu_{f_n}(t)) + \mathcal{H}_r\Phi_r(x_r, t) + \mathcal{F}_r x_r(t)). \tag{A2}$$

10991239, 2021, 6, Downloaded from https://onlinelibrary.wiley.com/doi/10.1002/rnc.5394 by University Of Maryland, Wiley Online Library on [05/03/2024]. See the Terms and Conditions (https://onlinelibrary.wiley.com/terms-and-conditions) on Wiley Online Library for rules of use; OA articles are governed by the applicable Creative Commons License

Now substituting the ISMC law (50) into the (A2)

$$\dot{V}_r(t) \leq \|S_r(t)\| \left((1 + \Delta_{max}\varsigma_o)(\|\nu_{f_l}(t)\| - \Gamma_r^*) + \|\mathcal{H}_r\Phi_r(x_r, t)\| - \|\nu_{f_l}(t)\|\right). \tag{A3}$$

Now choosing the modulation gain (54), (A3) becomes negative definite which satisfy the so-called reachability condition using (54).

10991239, 2021, 6, Downloaded from https://onlinelibrary.wiley.com/doi/10.1002/rnc.5394 by University Of Maryland, Wiley Online Library on [05/03/2024]. See the Terms and Conditions (https://onlinelibrary.wiley.com/terms-and-conditions) on Wiley Online Library for rules of use; OA articles are governed by the applicable Creative Commons License